JOURNAL OF THERMOPHYSICS AND HEAT TRANSFER
Vol. 30, No. 3, July-September 2016

# Master Equation Study of Vibrational and Rotational Relaxations of Oxygen

Daniil A. Andrienko* and Iain D. Boyd†
*University of Michigan, Ann Arbor, Michigan 48109*

DOI: 10.2514/1.T4769

**Transition rates in $O_2$–O collisions for each vibrational and rovibrational state are generated by means of the quasi-classical trajectory method using potential energy surfaces of different fidelities. The first potential energy surface, obtained via the double many-body expansion method, is adopted to obtain vibrational transition rates assuming transrotational equilibrium. The trajectory simulation on a simpler potential surface, based on the two-body pairwise interaction, generates a complete set of rates for each internal state. Vibrational and rotational relaxations of oxygen in a heat bath of parent atoms are modeled by a system of master equations at translational temperatures between 1000 and 20,000 K. It is shown that the vibrational relaxation becomes less efficient at high temperatures, in contrast with the conventional equation for relaxation time proposed by Millikan and White ("Systematics of Vibrational Relaxation," *Journal of Chemical Physics*, Vol. 39, No. 12, 1963, Paper 3209). Rotational and vibrational relaxation times are the same order of magnitude in the range of temperatures observed in hypersonic flows. The excitation of the vibrational mode in $O_2$–O collisions under typical postshock conditions occurs earlier than in other molecular systems. The exchange channel plays an important role in the internal energy randomization.**



## Nomenclature

| | | |
|---|---|---|
| $E_{\text{col}}$ | = | energy of collision, eV |
| $j, j'$ | = | initial and final rotational quantum numbers |
| $K$ | = | bound–bound transition rate, $\text{cm}^3/\text{s}$ |
| $n_i$ | = | number density of $O_2$ rovibrational level $i$, $\text{cm}^{-3}$ |
| $n_{\text{O}}$ | = | number density of atomic oxygen, $\text{cm}^{-3}$ |
| $T, T_{\text{vib}}$ | = | translational, vibrational, and rotational temperatures, K |
| $v, v'$ | = | initial and final vibrational quantum numbers |
| $\sigma$ | = | cross section, Å |
| $\tau_{\text{vib}}, \tau_{\text{rot}}$ | = | vibrational and rotational relaxation times, s |
| $\Phi$ | = | transition probability |

## I. Introduction

DURING flight at hypersonic speed, a significant degree of thermal nonequilibrium in the flow field can be observed. Because oxygen quickly dissociates during reentry, the $O_2$ thermochemistry has attained less attention than other aspects of hypersonic aerothermodynamics. However, during the cruise flight of a hypersonic vehicle at a moderate velocity of 2–3 km/s, a significant amount of molecular oxygen is encountered in the postshock region. Meanwhile, significant progress in the state-resolved chemistry models of atmospheric species has been achieved over the past decade [1–6]. Toward this end, the application of advanced numerical methods for the simulation of oxygen chemistry is described in the current work.

The quasi-classical trajectory (QCT) method was previously used to generate cross-section data for important three-body systems such as $N_2$–N, $N_2$–O, $O_2$–O, and $H_2$–H [5,7–9]. In these calculations, the simulation of atom–molecule collisions with randomly sampled parameters is preceded by the choice of an accurate, preferably ab initio, potential energy surface (PES), which ultimately governs the properties of molecular systems. Further analysis should involve the solution of kinetic equations that are coupled to the set of state-specific transition rates. This step presents a significant computational challenge due to the large number of internal states. An accurate state-to-state model considers each energy state as a separate species. The total number of equations is on the order of several thousand for each molecular species, and such a system of equations is numerically stiff due to the rapid dissociation at high temperatures.

These factors make the state-to-state kinetic approach an extremely expensive and, at the same time, very desirable technique, since it is possible to model the thermal nonequilibrium in a shock flow without assuming the existence of internal temperature. Recent works in this direction have reported the studies of rovibrational relaxation and dissociation in the $N_2$–N [3,4] and the $O_2$–Ar [10] systems using accurate transition rates under constant heat bath conditions. Among other molecular systems, the interaction of $O_2$ with its parent atom is of interest [11]. Oxygen chemistry is also important in the flight environment of scramjet engines. On the other hand, vibrational relaxation in $O_2$–O collisions is known to proceed several orders of magnitude faster than that of other molecules [12] due to the large attractive component in the $O_3$ potential energy surface [13].

Recently, the importance of using a state-resolved kinetic approach for the description of oxygen shock flows was demonstrated [14]. The $O_2$–O transition rates, obtained in the present work via the Varandas and Pais PES [13], were used to simulate the vibrational relaxation in the range of translational temperatures between 4000 and 10,800 K in experiments conducted by Ibraguimova et al. [15]. Since the complete set of $O_2-O_2$ transition rates obtained by trajectory simulations is not available, the force harmonic oscillator model was used [16]. The state-to-state approach was shown to give a consistently more accurate representation of vibrational temperature behind the shock, measured by laser absorption in the $O_2(X^3\Sigma_g^- - B^3\Sigma_u^-)$ Schumann–Runge bands, compared to the two-temperature model [17]. The difference between these two thermodynamic models increases with temperature, which is due to the larger amount of atomic oxygen in the stronger shock waves.

The $O_2-O$ transition rates for each vibrational state were obtained previously by Esposito et al. [5] on an accurate PES by Varandas and Pais [13] at temperatures between 100 and 10,000 K. The present paper adopts two potential energy surfaces of different fidelity. First, the $O_2-O$ system is revisited using the same PES as in [5] over a broader range of collision energy that is of relevance to hypersonic flows. Due to the high cost of employing this PES, the rates are obtained for each vibrational state assuming transrotational

Received 18 May 2015; revision received 28 September 2015; accepted for publication 1 November 2015; published online 8 January 2016. 

*Postdoctoral Research Fellow, Department of Aerospace Engineering, 1320 Beal Ave.

†James E. Knott Professor, Department of Aerospace Engineering, 1320 Beal Ave.

equilibrium. Additionally, a complete set of trajectory simulations for each internal state is carried out on a simpler PES, based on the pairwise potential. These two sets of rates are employed in a system of master equations to describe the rotational and vibrational relaxation in $O_2$–O collisions.

This paper is organized as follows. Section II provides a background on the molecular structure of oxygen and on the existing data of $O_2$–O collisional dynamics. Section III addresses the governing relations of the QCT method and master equations. The detailed study of rovibrational relaxation is presented in Sec. IV. Conclusions are given in Sec. V. The supplemental data are listed in the Appendix.

## II. Background

### A. $O_2$ and $O_3$ Molecular Structure

In the present work, two potential energy surfaces of different fidelity are adopted to study the $O_3$ system. The first PES is obtained by the summation of interactions between each pair of atoms. This potential surface does not account for the many-body interaction; however, the QCT simulation with this PES can demonstrate the influence of the three-body interaction. This potential surface is obtained as follows:

$$V_{O_3}(r_{AB}; r_{BC}; r_{AC}) = V_{O_2,AB}(r_{AB}) + V_{O_2,BC}(r_{BC}) + V_{O_2,AC}(r_{AC}) \quad (1)$$

where the diatomic interaction $V_{O_2}(r)$ is given by the Hulburt–Hirschfelder (HH) potential:

$$V_{O_2}(r) = D[(1 - \exp(-a(r - r_e)))^2 + ca^3(r - r_e)^3 \exp(-2a(r - r_e))(1 + ab(r - r_e))] \quad (2)$$

Coefficients $a$, $b$, and $c$ are determined by the spectroscopic constants of oxygen, listed in [18]. The Wentzel–Kramers–Brillouin (WKB) method is used to generate energy levels. The HH PES supports 36 vibrational states, a maximum of 231 rotational states, and a total number of 5117 rovibrational states of $O_2(X^3\Sigma_g^-)$.

An accurate $O_3(X^1A_1)$ PES [13], derived via the double many-body expansion method, is also adopted for the purpose of high-fidelity simulation. This PES is obtained by the multiproperty fitting of ab initio energies, existing experimental data on total scattering cross sections, and the measurements of kinetic thermal rates. The Varandas and Pais PES [13] well describes the main topographical features of the singlet ozone as a whole and presents a good compromise between cost and accuracy [19,20]. The Varandas and Pais PES [13] reproduces the ab initio value of energy difference between open chain stable and cyclic metastable conformers and has the $R^{-n}$ function of long-range forces in the dissociation channel. The $O_3$ dissociation energy of 1.13 eV at the O–O bond length of 1.27 Å and the angle of 116.8 deg are in excellent agreement with experimental data [21].

The extended Hartree–Fock approximate correlation energy method [22] is used to described the two-body potential in the Varandas and Pais PES [13]. The WKB method generates 47 vibrational levels and a maximum of 236 rotational levels for molecular oxygen on this PES. Internal energies for these PESs are given in [23]. The total number of rovibrational states on the Varandas and Pais PES [13] is equal to 6245. Taking into account the nuclear spin statistics of a homonuclear molecule, the even-numbered rotational levels for the $O_2(X^3\Sigma_g^-)$ state are forbidden. Since, during a bound–bound rovibrational transition, the symmetry of the initial and final states cannot change, transitions of the $O_2$ molecule in the ground electronic state are only allowed between odd-numbered rotational levels [21].

When incorporated into the QCT code, the Varandas and Pais PES [13] requires approximately 8 to 10 times more computational resources than the HH PES. Due to this reason, the calculation of state-specific transition rates for the entire rovibrational ladder using the Varandas and Pais PES [13] is now in progress and not reflected in the present paper. As the first step of investigation using the high-fidelity PES, the rotationally averaged transition rates for all vibrational states are obtained at rotational temperatures of 1000, 2000, 3000, 5000, 10,000, and 20,000 K. For the HH PES, a complete set of rovibrational cross sections is generated and discussed in the present paper.

The comparison of HH and Varandas and Pais [13] potentials is shown in Fig. 1 for the $O_2$–O collinear collision. The HH PES suggests a deep triangular minimum of potential energy, whereas the PES by Varandas and Pais has a linear direction of the closest approach and two saddle points at distances of 1.6 and 2.4 Å. The potential barriers, introduced by these saddle points, are 0.6 and 1.9 eV, respectively. Thus, it is expected that transition rates obtained using the HH PES will be higher than those obtained with the Varandas and Pais [13] potential.

### B. Previous Experimental and Theoretical Studies

The vibrational relaxation of air species is usually described by the Millikan–White (MW) equation that connects the vibrational relaxation time to the macroscopic parameters, such as temperature and pressure. In the original work [24], the analysis of a large amount of experimental data was performed. It was found that vibrational relaxation becomes more efficient as gas temperature increases. The typical relaxation times of nitrogen and oxygen species vary from $10^{-3}$ to $10^{-7}$ atm · s in the range of temperatures from 1000 to 8000 K. However, there are several exceptions to this rule, when the

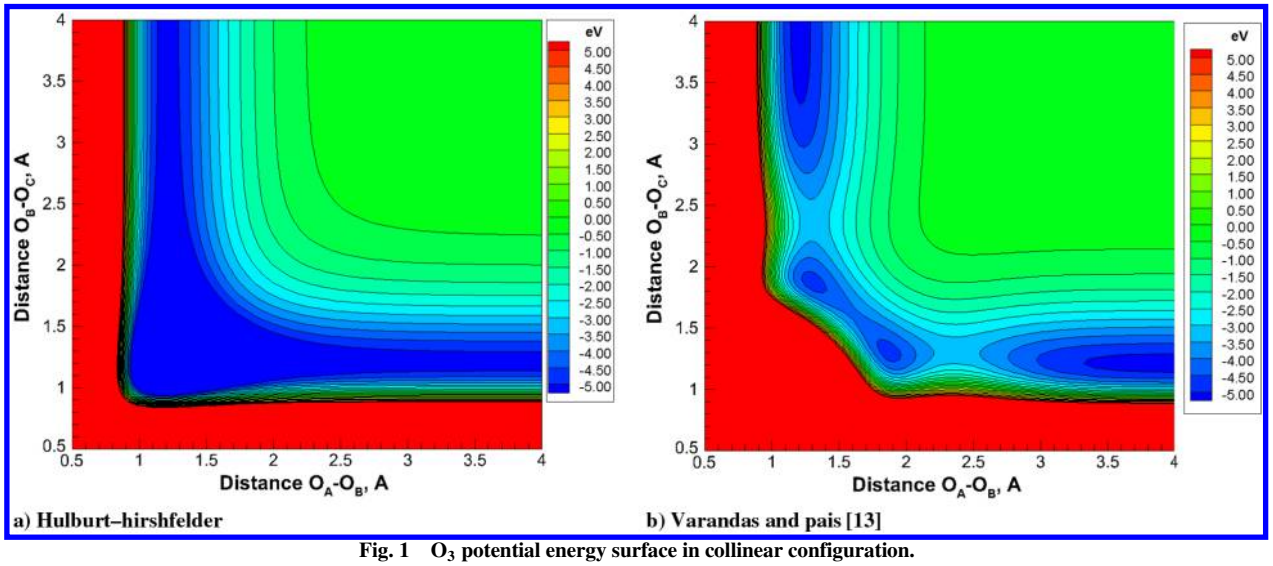


**Fig. 1 $O_3$ potential energy surface in collinear configuration.**

vibrational relaxation of some species proceeds much faster. For example, the relaxation in NO–NO, $O_2$–O, and $N_2$–O collisions occurs two to three orders of magnitude faster than in other types of collisions. The experimental data on such molecular systems are scarce [25–27] and cover only a narrow temperature range below 4000 K.

The vibrational relaxation time in $O_2$–O collisions at high temperatures was measured in experiments only by Kiefer and Lutz [28] and Breen et al. [27] using two different techniques. In the former work, atomic oxygen was generated before the vibrational relaxation by the thermal decomposition of ozone. Later, Breen et al. measured the "Napier" vibrational relaxation time [29] in the shock relaxation zone. In this case, a RF discharge was used to generate atomic oxygen in the $O_2$–Ar mixture and in pure $O_2$. Both works reported similar results; however, a substantially different temperature dependence of vibrational relaxation time was found.

According to [28], fast vibrational relaxation in $O_2$–O collisions is the evidence of a strong chemical effect between the target and projectile particles. Breen et al. [27] and Breig [30] suggested that the efficient energy exchange was due to the large attractive component in the three-body potential. Quack and Troe [12] employed the statistical adiabatic channel model and confirmed these results. Unfortunately, due to the lack of computational resources at that time, the investigation of $O_2$–O collision dynamics was performed in a limited manner, leaving the problem of accurate state-to-state thermodynamic models unaddressed.

The analysis of microscopic parameters, such as collision duration and number of interatomic vibrations in the $O_2$–O interaction, was performed in [31]. It was shown that an efficient energy exchange occurs via the strongly coupled complex formed between the projectile and target particles. The randomization of vibrational energy takes place at kinetic energies as low as 0.05 eV, particularly because of the deep potential well in the intermediate $O_3$ molecule. At larger collision energies, vibrationally inelastic collisions are less probable. An approach, similar to [31], was adopted in [32] to analyze the vibrational deactivation rate at different kinetic temperatures. It was found that the vibrational deactivation is more efficient at low temperatures (500–2000 K) rather than at the high-temperature limit.

## III. Governing Equations

### A. QCT Method

A trajectory of the target molecule and projectile atom is described by a system of first-order partial differential equations:

$$\begin{cases} \dot{q}_i = \frac{\partial H}{\partial p_i}, \\ \dot{p}_i = -\frac{\partial H}{\partial q_i}, \quad i = 1,2,3 \end{cases} \tag{3}$$

where $q = \{q_i, Q_i\}$ are the generalized coordinates; $p = \{p_i, P_i\}$ are the conjugate momenta of the molecule and atom–molecule system, respectively; and $H$ is the total Hamiltonian [33]. The continuous range of translational energy from $10^{-3}$ to 18 eV is studied. Stratified sampling is applied to integrate the transition probability over the impact parameter. The size of the bin is $2 \times 10^3$ trajectories per impact parameter per collision energy. An error analysis is performed for each trajectory by comparing the initial and final total energies. The initial rovibrational state of the target molecule is assigned to a constant for each batch when computing the bound–bound rovibrational transition probability. In the case when only transvibrational cross sections are of interest, the initial rotational state is chosen randomly according to the Boltzmann distribution. The internuclear distance $r_{BC}$ is sampled according to the approach proposed in [34]. The solution of Eq. (3) is obtained by the 11th-order-accurate Adams–Bashfort–Moulton method [35] with a variable time step. An averaged probability $\bar{\Phi}$ of the bound–bound transition from the initial state $(v, j)$ at translational energy $E_{col}$ is computed as follows:

$$\bar{\Phi}(E_{col}, v, j) = \frac{1}{(2\pi)^3 b_{max}^2} \int_{b=0}^{b_{max}} \int_{\theta=0}^{\pi} \int_{\varphi=0}^{2\pi} \int_{\eta=0}^{2\pi} \int_{\xi=0}^{2\pi} b\Phi(E_{col}, b, \theta, \varphi, \eta, \xi) \times \sin(\theta)\, db\, d\theta\, d\varphi\, d\eta\, d\xi \tag{4}$$

where $(v, j)$ are the initial vibrational and rotational quantum numbers; the transition probability $\Phi$ is sampled over the impact parameter $b$, orientation angles $\theta$ and $\varphi$, orientation $\eta$ of the angular momentum, and initial vibrational phase angle $\xi$ of the target molecule; and $b_{max}$ is the impact parameter at which only elastic collisions occur. The cross section of the bound–bound transition $(v, j) \to (v', j')$ is calculated as follows:

$$\sigma(E_{col}, v, j \to v', j') = \pi b_{max}^2 \bar{\Phi}(E_{col}, v, j \to v', j') \tag{5}$$

where $(v', j')$ are the final vibrational and rotational quantum numbers. Sometimes, it is convenient to perform analysis assuming transrotational equilibrium. In this case, the state-specific cross section, given by Eq. (5), should be summed over all rotational states of the final vibrational state. The cross section of the transition $(v, j) \to v'$ is derived as follows:

$$\sigma(E_{col}, v, j \to v') = \sum_{j'} \sigma(E_{col}, v, j \to v', j') \tag{6}$$

Now, the cross section of the $v \to v'$ transition is found by averaging the cross section in Eq. (6) over the initial rotational state, assuming that they are populated according to the Boltzmann distribution with $T_{rot} = T$:

$$\sigma(E_{col}, v \to v') = \frac{\sum_j g_j \exp(-(e_{v,j} - e_{v,0})/k_B T) \sigma(E_{col}, v, j \to v')}{\sum_j g_j \exp(-(e_{v,j} - e_{v,0})/k_B T)} \tag{7}$$

where $g_j = (2j + 1) \bmod (j, 2)$ is the rotational degeneracy of the state $(v, j)$ in the $O_2$ ground electronic state. The decomposition of internal energy into vibrational and rotational contributions in Eq. (7) takes the following form: $e_{vib,i} = e_{v,0}$ and $e_{rot,i} = e_{v,j} - e_{v,0}$. Then, the rotationally averaged rate of transition $v \to v'$ is calculated as follows:

$$K(T, v \to v') = \frac{8\pi}{\sqrt{\mu_{A,BC}}} (2\pi k_B T)^{-3/2} \times \int_{E_{col}=0}^{\infty} \sigma(E_{col}, v \to v') E_{col} \exp\left(\frac{-E_{col}}{k_B T}\right) dE_{col} \tag{8}$$

The rate of the rotationally resolved bound–bound transition $(v, j) \to (v', j')$ can be calculated in a manner similar to Eq. (8):

$$K(T, v, j \to v', j') = \frac{8\pi}{\sqrt{\mu_{A,BC}}} (2\pi k_B T)^{-3/2} \times \int_{E_{col}=0}^{\infty} \sigma(E_{col}, v, j \to v', j') E_{col} \exp\left(\frac{-E_{col}}{k_B T}\right) dE_{col} \tag{9}$$

The principle of detailed balance is invoked to obtain the rates of endothermic bound–bound transitions in order to reduce the statistical error:

$$K(T, v', j' \to v, j) = K(T, v, j \to v', j') \frac{Q_{v,j}(T_{rot}, T_{vib})}{Q_{v',j'}(T_{rot}, T_{vib})} \tag{10}$$

where

$$Q_{v,j}(T_{rot}, T_{vib}) = (2j+1) \exp[-(e_{v,j} - e_{v,0})/k_B T_{rot}] \exp[-e_{v,0}/k_B T_{vib}]$$

Thermal equilibrium is assumed in Eq. (10): $T_{rot} = T_{vib} = T$. The reaction rate, given by Eq. (9), has to be modified to account for the

degeneracy of reactants and PES. For the bound–bound transition, induced by the collision of $O(^3P)$ and $O_2(^3X_g^-)$, the spin and orbital degeneracy factor can be expressed in the form given in [36]:

$$\frac{1}{g_{BB}} = 3\left(5 + 3\exp\left(-\frac{227.6}{T}\right) + \exp\left(-\frac{325.9}{T}\right)\right) \tag{11}$$

where the factor of three corresponds to the $O_2$ triplet state. The expression in parentheses describes the degeneracy of $O(^3P_J)$, where $J = 0$, 1, and 2. Now, the degeneracy factor of the bound–bound transition is found as a ratio of the PES degeneracy to the degeneracy of reactants. Taking into account that the PES of $O_3$ in the ground electronic state is nondegenerate, the total degeneracy is given by Eq. (11). At high temperatures, the degeneracy factor asymptotically approaches a value of 1/27.

### B. Master Equations

At low kinetic temperatures, the population of rovibrational states converges to equilibrium significantly faster than the dissociation process takes place [3,37]. At higher temperatures, dissociation and thermal relaxation occur within the same timescale, and these processes have to be studied in a coupled manner. In the present paper, vibrational relaxation is studied at temperatures ranging from 500 to 20,000 K. Strictly speaking, the simulation of heat bath conditions should include the molecular depletion; however, the dissociation is artificially excluded from the present study in order to focus on the state-resolved thermalization. Omitting the dissociation and recombination processes, the vibrational and rotational relaxations of oxygen can be studied by considering only bound–bound transitions. The resulting master equation for the number density of rovibrational level $i$ can be written as follows:

$$\frac{dn_i}{dt} = \sum_{i' \neq i}(K(T, v', j' \to v, j)n_O n_{i'} - K(T, v, j \to v', j')n_O n_i),$$
$$i = 1, \ldots, N_s, \qquad i' = 1, \ldots, N_s \tag{12}$$

where $N_s$ is the total number of rovibrational states. The rates of bound–bound transitions are given by Eq. (9). Equation (12) describes the rotational-vibrational-translational (RVT) energy transfer and is termed as the RVT model. An implicit method of third-order accuracy for diagonal and second-order accuracy for offdiagonal elements is applied to integrate Eq. (12). The initial number density, given by $n_{O_2,0} + n_{O,0}$, is set to $10_{18}$ cm$^{-3}$. This is equivalent to a pressure of 1.3626 atm at a gas temperature of 10,000 K. No mass exchange with the surrounding medium is allowed. To simulate conditions when the atom–molecule collisions are dominant, the initial number density of atomic oxygen is set to $\alpha = 0.99$ of the total number density. At initial nonequilibrium conditions, the population of the rovibrational states is given by the Boltzmann distribution with the temperature $T_0 = 100$ K, as follows from Eq. (13):

$$n_{v,j,0} = \frac{Q_{v,j}(T_{rot}, T_{vib})}{\sum_i Q_{v,j}(T_{rot}, T_{vib})} n_{O_2,0} \tag{13}$$

where $n_{O_2,0}$ is the total number density of oxygen. The initial internal temperatures, $T_{rot,0}$ and $T_{vib,0}$, are equal to $T_0$ for the RVT model.

The system of governing equations in the case of transrotational equilibrium has the following appearance:

$$\frac{dn_i}{dt} = \sum_{i' \neq i}(K(T, v' \to v)n_O n_{i'} - K(T, v, \to v')n_O n_i),$$
$$i = 0, \ldots, N_v, i' = 0, \ldots, N_v \tag{14}$$

where $N_v$ is the total number of vibrational states, and transition rates are given by Eq. (8). Equation (14) describes the vibrational-translational (VT) energy transfer and is termed as the VT model. The initial rotational temperature is set to the heat bath temperature, and the initial vibrational temperature is set to $T_0$ for the VT model.

## IV. Results

### A. Verification of VT Rates

The mono- and multiquantum vibrational deactivation rates, averaged at the rotational temperature $T_{rot} = T$ in the range between 1000 and 10,000 K, are shown in Figs. 2a and 2b, respectively. Monoquantum transition rates from $v = 1$, 10, and 20, obtained using the HH PES, are given by solid lines. The rates, obtained by the Varandas and Pais PES [13], are shown with symbols, and rates from [11] are given by dashed lines. A similar notation is adopted in Fig. 2b for transitions of $v = 10$ and 20 with $\Delta v = 10$ and $v = 30$ and 40 with $\Delta v = 30$.

The difference between the HH and Varandas and Pais [13] rates is the largest at low temperatures. As expected, the influence of the three-body interaction term is the most significant under these conditions. The discrepancy diminishes at high temperatures. The maximum difference is on the order of two to four times at a temperature of 1000 K.

The present VT rates, obtained using the Varandas and Pais PES [13], are in a very good agreement with those reported in [11]. One can see a disagreement at the high-temperature limit ($T = 10{,}000$ K), which is explained by the insufficient upper limit

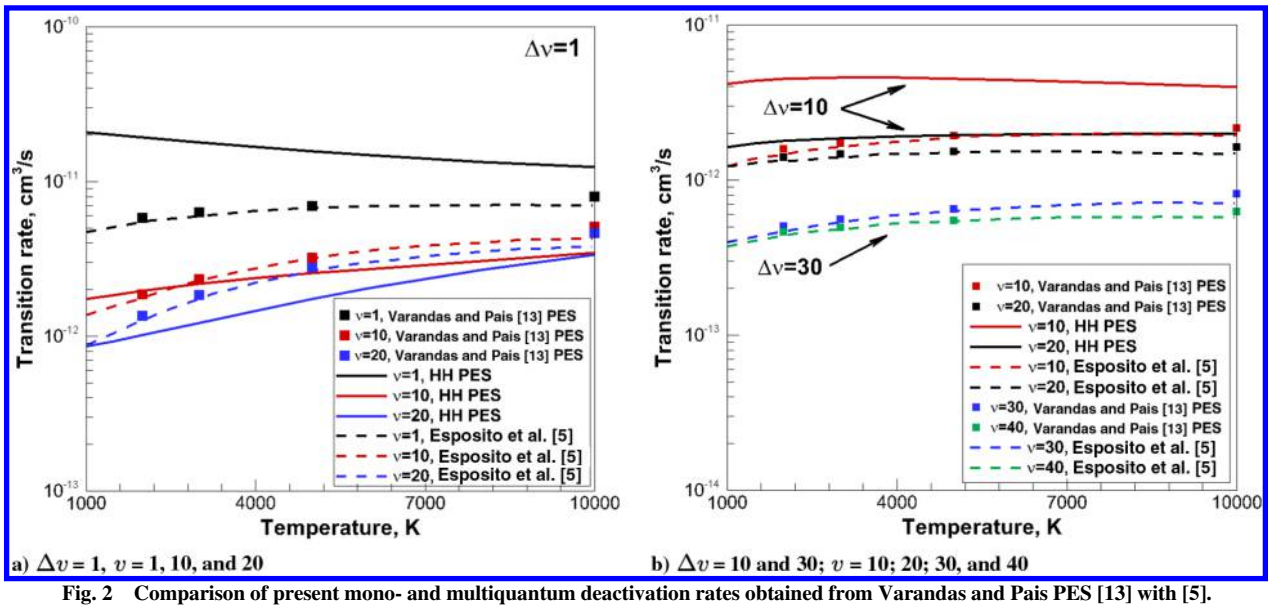


**Fig. 2 Comparison of present mono- and multiquantum deactivation rates obtained from Varandas and Pais PES [13] with [5].**

of energy scale adopted in the Esposito and Capitelli calculations [11]. In the original paper [11], the maximum of the kinetic energy was set to 3 eV; whereas in the present work, calculations at $T = 10{,}000$ K are conducted up to 6.5 eV. The overall discrepancy due to the narrow energy scale reaches a maximum of 18%.

From Fig. 2, it follows that the variation of VT rates is relatively small over the wide temperature range. This is also true for the large multiquantum transitions. Meanwhile, the rate of monoquantum deactivation from $v = 1$, shown in Fig. 2a by dashed lines, only slightly increases toward high temperatures, suggesting that the relaxation time may also increase with the temperature. It is interesting to compare the present results to the transition rates observed in collisions of oxygen with an inert atom, such as argon [10]. The comparison of vibrationally resolved VT rates, generated in the present work by the QCT method, is shown in Figs. 3a and 3b for the $O_2$–O and $O_2$–Ar systems, respectively.

In both cases, the VT transition rates are obtained for each combination of initial and final vibrational states by summation over final rotational state $j'$, compatible with $v'$, and averaging over initial rotational state at transrotational temperatures of 2000, 3000, 5000, and 10,000 K. The lowest temperature corresponds to the lowest surface. The rates on the left of the peak correspond to exothermic transitions. The rates of endothermic transitions, calculated using the principle of detailed balance, are shown on the right of the peak. One can see a very weak dependence of $O_2$–O rates of exothermic transitions on temperature, whereas the efficiency of vibrational deactivation in $O_2$–Ar collisions strongly depends on the translation temperature. Moreover, there is a small variation of $O_2$–O exothermic rates with the initial vibrational quantum number. The present results demonstrate a small decrease of $O_2$–O VT rates at very high vibrational levels due to the dissociation channel. The weak dependence of rates on temperature and $v$ can be attributed to the short memory about the initial state due to the strong energy randomization via the large attractive component of the $O_3$ PES [32]. On the other hand, $O_2$−Ar vibrational deactivation rates strongly depend on $v$.

### B. VT and RVT Models

The solution of Eq. (12) describes a time-dependent population of each rovibrational level during the relaxation to thermal equilibrium. Because the large number of states complicates further analysis, the energy-equivalent rotational and vibrational temperatures are used to describe the population of the entire rovibrational ladder. The average vibrational and rotational energies are evaluated in the following manner:

$$\bar{e}_{\text{vib}} = \frac{\sum_i e_{\text{vib},i} n_i}{\sum_i n_i} \tag{15}$$

$$\bar{e}_{\text{rot}} = \frac{\sum_i e_{\text{rot},i} n_i}{\sum_i n_i} \tag{16}$$

Due to the centrifugal forces arising from the rotation of a molecule, the vibrational and rotational levels of energy are coupled. To perform an appropriate sampling of trajectories in the QCT method, the energy of the internal degrees of freedom should be decoupled. In the present work, the "vibration-prioritized" framework [3,38] is adopted. The energy of a vibrational state is calculated as the energy of the rovibrational state with $j = 0$, whereas the energy of a rotational state is obtained as the difference between the rovibrational and vibrational energies. The rotational and vibrational temperatures are evaluated from $\bar{e}_{\text{rot}}$ and $\bar{e}_{\text{vib}}$ by solving the following implicit equations:

$$\bar{e}_{\text{vib}} = e_{\text{vib}}(T_{\text{vib}}) \tag{17}$$

$$\bar{e}_{\text{rot}} = e_{\text{rot}}(T_{\text{rot}}, T_{\text{vib}}) \tag{18}$$

where

$$e_{\text{rot}}(T_{\text{rot}}, T_{\text{vib}}) = \frac{\sum_i e_{\text{rot},i} Q_i(T_{\text{rot}}, T_{\text{vib}})}{\sum_i Q_i(T_{\text{rot}}, T_{\text{vib}})}, \qquad i = 1, \ldots, N_s \tag{19}$$

$$e_{\text{vib}}(T_{\text{vib}}) = \frac{\sum_v e_{v,0} Q_v}{\sum_v Q_v}, \qquad v = 0, \ldots, N_v \tag{20}$$

In Eq. (20), $Q_v$ is the statistical weight of vibrational state $v$. The solution of Eqs. (17) and (18) is obtained by the bisection method. It is important to note that the vibrational and rotational temperatures, defined by Eqs. (17–20), are involved only in the postprocessing step, after the solution of the master equations has been obtained. The evolution of vibrational temperature, computed under the heat bath conditions at $T = 1000$, 5000, and 10,000 K using rates corresponding to the HH PES, is shown in Fig. 4a. Solid and dashed lines correspond to the RVT and VT models, respectively. For the entire range of translational temperatures, the VT model predicts faster vibrational relaxation than the RVT model. This difference is caused by a significant rotational nonequilibrium in $O_2$–O collisions. In fact, as will be shown later, the vibrational relaxation in the collision of oxygen with the parent atom is only slightly faster than the rotational relaxation.

A comparison of VT models using two sets of reaction rates from the HH and Varandas and Pais PESs [13] is shown in Fig. 4b. As one can see, the solution of master equations using the Varandas and Pais PES [13] predicts slower relaxation of vibrational energy than that by the HH PES. This result is expected from the general behavior of the VT rates in Fig. 2. It is worth noting that the difference in the vibrational relaxation time becomes smaller as the translational temperature increases because, at these conditions, colliding particles interact mostly via the repulsive part of the potentials.

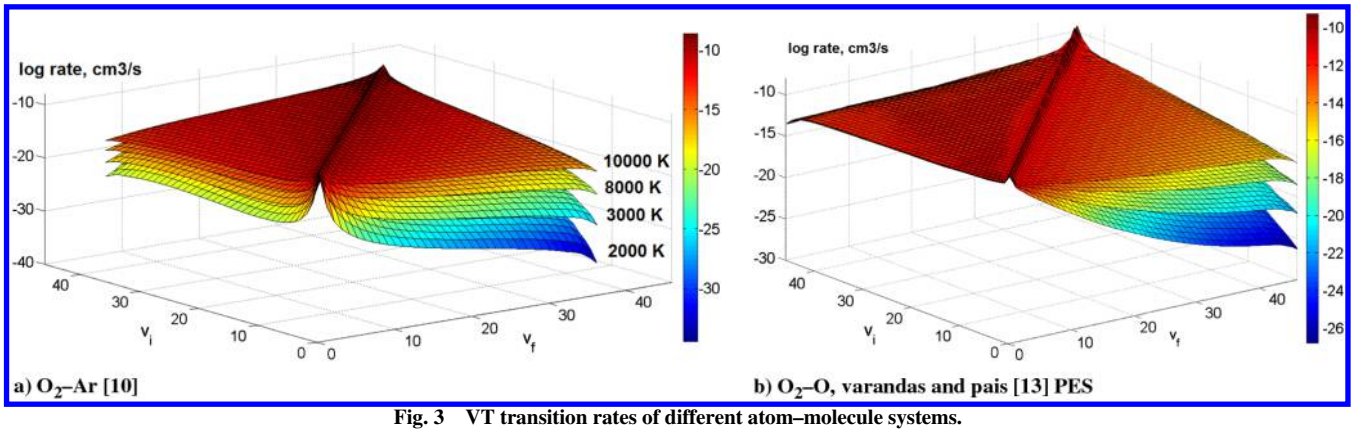


**Fig. 3 VT transition rates of different atom–molecule systems.**

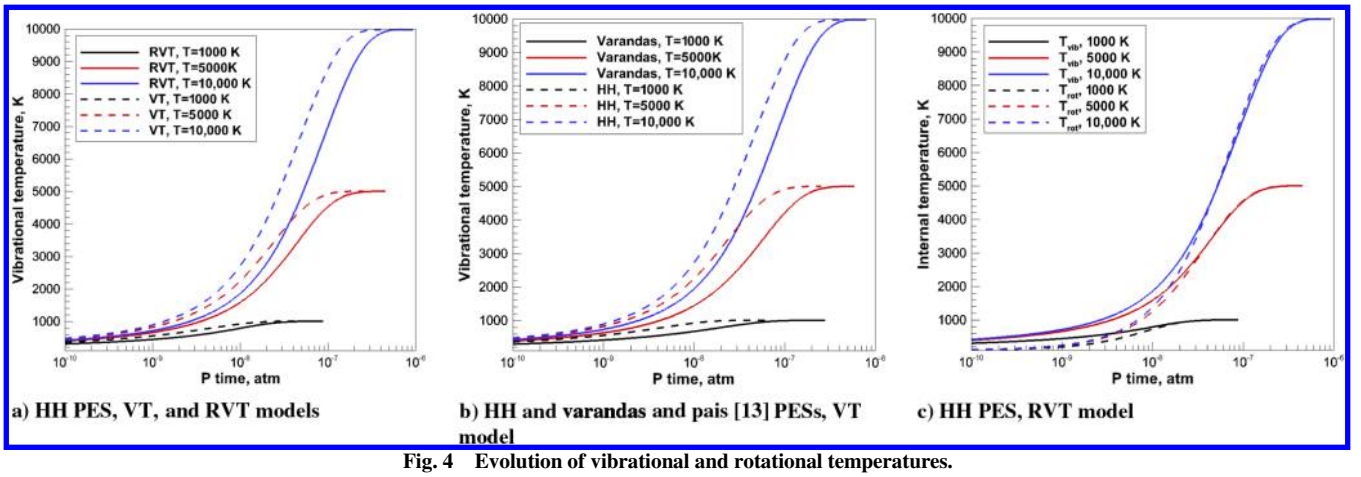


**Fig. 4 Evolution of vibrational and rotational temperatures.**

The evolution of vibrational and rotational temperatures, given by the RVT model using rates from the HH PES, is shown in Fig. 4c. In the range of heat bath temperatures between 1000 and 10,000 K, a significant degree of vibrational and rotational nonequilibrium is observed. The latter explains the difference in $T_{\text{vib}}$ given by the VT and RVT models in Fig. 4a. At the early stage of relaxation, the rotational temperature is always lower than the vibrational temperature. This situation is also observed for $N_2$–N collisions [3]. Eventually, the rotational temperature becomes greater than $T_{\text{vib}}$ at the late stage of relaxation. During the quasi-stationary relaxation phase, when modeling dissociation and recombination, the rotational temperature is always larger than the vibrational temperature. This feature is left for further investigation.

It is possible to define the vibrational and rotational relaxation times based on the temporal evolution of internal energy. There are several ways to define a characteristic relaxation time [39]. One of the ways is to calculate the relaxation time as if the equilibration process follows the Landau–Teller (LT) equation:

$$\frac{\mathrm{d}e_{\text{vib}}(t)}{\mathrm{d}t} = \frac{e_{\text{vib}}(t,T) - e_{\text{vib}}(t,T_{\text{vib}})}{\tau_{\text{vib}}} \tag{21}$$

The vibrational energy, given by Eq. (21), evolves exponentially in time. The vibrational relaxation time $\tau_{\text{vib}}$ is then defined by the corresponding vibrational energy $e_{v,\text{efold}}$:

$$e_{\text{vib,efold}} = \frac{1}{e}e_{\text{vib}}(T_0) + \left(1 - \frac{1}{e}\right)e_{\text{vib}}(T) \approx 0.3679 \times e_{\text{vib}}(T_0) + 0.6321 \times e_{\text{vib}}(T) \tag{22}$$

where $e_{\text{vib,efold}}$ is the average vibrational energy at time $\tau_{\text{vib}}$; and $e_{\text{vib}}(T_0)$ and $e_{\text{vib}}(T)$ are the average vibrational energies evaluated at initial and final temperatures, respectively. This approach is called the e-folding method [39]. The rotational relaxation time is calculated in a similar way.

The present rotational and vibrational relaxation times are shown in Fig. 5. Lines with square and delta symbols correspond to $\tau_{\text{vib}}$ obtained by the VT model, using the HH and Varandas and Pais PESs [13], respectively. The lines with right and left triangles correspond to $\tau_{\text{vib}}$ and $\tau_{\text{rot}}$ obtained by the RVT model from the HH PES, respectively. Circle and diamond symbols represent the vibrational relaxation time measured in experiments by Breen at al. [27] and Kiefer and Lutz [28], respectively. The dashed–dotted line corresponds to the curve fit of vibrational relaxation time using the MW relation to the data from [28].

The vibrational relaxation time obtained from the VT model and the Varandas and Pais PES [13] is in good agreement with the existing experimental data in the range from 1000 to 3600 K. Both $\tau_{\text{vib}}$, obtained from the Varandas and Pais [13] and HH PESs, have a positive temperature slope, which corresponds to the observation made by Breen at al. [27]. The agreement with the earlier measurements by Kiefer and Lutz is less successful [28]. The largest difference is observed in the high-temperature region and is not higher than 15%. Taking into account the overall uncertainty of the shock tube facility, the agreement with the experimental data is very satisfactory. To the authors' knowledge, other experimental data on the $O_2$–O relaxation in this temperature range, as well as other simulations that adopt a master equation, do not exist.

The direct extrapolation of vibrational relaxation time by Kiefer and Lutz [28] outside of the experimental range by using the MW relation (dashed–dotted line in Fig. 5) shows a significant difference from the present models based on either Varandas and Pais [13] or HH potentials. The MW expression suggests that the vibrational relaxation of oxygen by the parent atom becomes more efficient with temperature [40]. The present results support a directly opposite trend: the vibrational relaxation time becomes smaller at low temperatures. The increase of vibrational relaxation time with temperature can be attributed to a strong chemical effect in the $O_3$ system due to the large attractive component in the PES [41]. This observation is in agreement with the results by Quack and Troe [12], obtained by means of the statistic adiabatic channel model.

Both the RVT and VT vibrational relaxation times based on the HH PES are smaller than the relaxation time from the Varandas and Pais PES [13]. This result demonstrates the influence of the three-body interaction in the $O_2$–O collisions. The HH PES has a deeper and broader potential well, compared to the Varandas and Pais PES [13], as can be seen in Fig. 1. This results in a stronger randomization of internal energy [31]. The agreement of the RVT HH vibrational relaxation time with the experimental data is very good; however, one

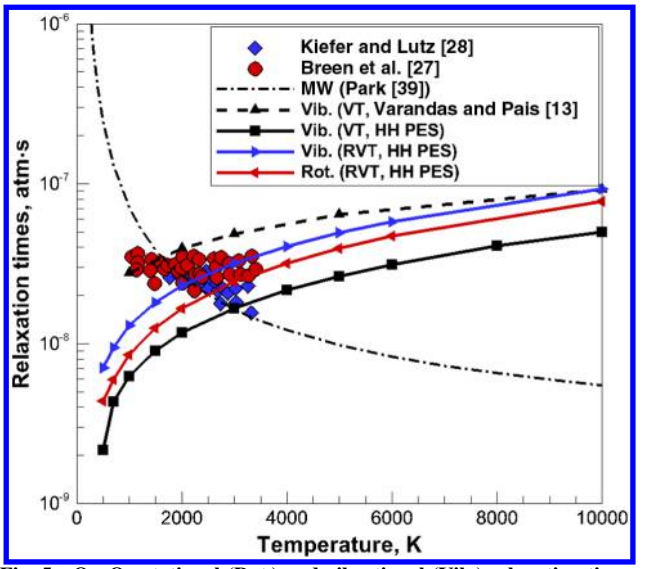


**Fig. 5 $O_2$–O rotational (Rot.) and vibrational (Vib.) relaxation times, given by master equations on Varandas and Pais [13] and HH PESs.**

should keep in mind that no $O_2-O_2$ collisions are included in the present simulation. Thus, the actual RVT vibrational relaxation time in the $O_2-O$ mixture may be different from that reported in the present work.

Another interesting feature of the present results is the strong coupling between the vibrational and rotational relaxations. The results by the RVT model suggest that the rotational relaxation is only slightly faster than the vibrational relaxation in the range of temperatures from 500 to 10,000 K. The linking between $\tau_{vib}$ and $\tau_{rot}$ explains the large difference in the vibrational temperature obtained by means of the VT and RVT models in Fig. 4a. The presence of rotational nonequilibrium at high temperatures is in agreement with recent QCT simulations of other molecular systems [4,10]. However, at low temperatures, the conventional assumption is that the rotational relaxation occurs much faster than thermalization of vibrational degrees of freedom [3], which is profoundly different from what is observed in $O_2$–O collisions. The similar values of $\tau_{rot}$ and $\tau_{vib}$ for $O_2$–O cause the concurrent rotational and vibrational nonequilibria, as follows from Fig. 4c.

The results of the VT model using the Varandas and Pais PES [13] are compared to the vibrational relaxation time derived from the rate of monoquantum deactivation and to that reported by Esposito et al. [5] and Ibraguimova et al. [15] in Fig. 6. The curve with triangles and the curve with squares describe the vibrational relaxation time by the VT model and the corresponding rate of monoquantum deactivation from $v = 1$. Circle symbols correspond to the experimental data from [27]. The relaxation time, given by the dashed line, is taken from the experimental work [15]. The solid line represents the relaxation time derived from the rate of monoquantum deactivation by Esposito and Capitelli [11]. The dashed–dotted line and square symbols represent Park's [17] curve fit and the theoretical data by Quack and Troe [12]. Experimental measurements by Kalogerakis et al. [42] and Pejaković et al. [43] at room temperature are given by right and left triangles, respectively.

The results by Ibraguimova et al. [15] were obtained by measuring the vibrational temperature behind the shock waves in pure oxygen in the range of postshock temperatures between 4000 and 10,800 K. The experimental data on the absorption of laser radiation in the Schumann–Runge bands were interpreted in terms of vibrational temperature. The vibrational relaxation time was then fitted to the general form, given by the Landau–Teller theory [44] for the best description of $T_{vib}$ using the two-temperature model. The following equation was used to obtain $\tau_{vib}$:

$$P\tau_{vib} = \frac{kT}{P_{10}\sigma_0}\sqrt{\frac{\pi\mu}{8RT}}\frac{1}{1-\exp(-\theta/T)}, \qquad Pa-s \qquad (23)$$

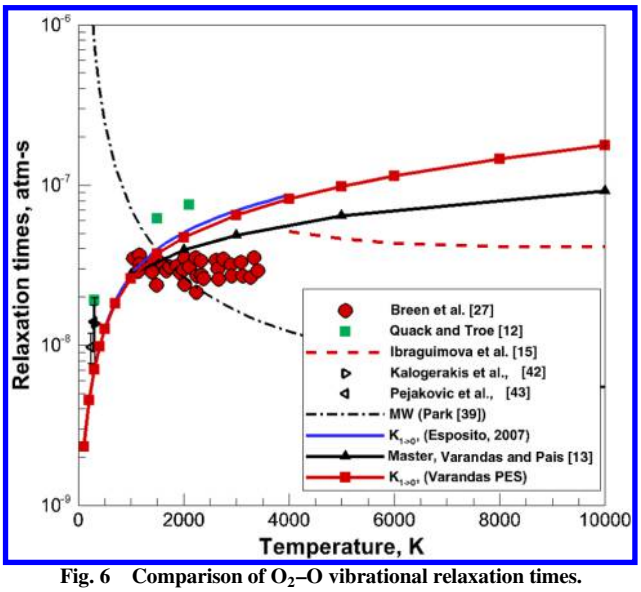


**Fig. 6 Comparison of $O_2$–O vibrational relaxation times.**

**Table 1 Curve fit parameters of relaxation times**

| | *A* | *B* | *C* | *D* |
|---|---|---|---|---|
| $P\tau_{vib}$, RVT, HH PES | $-3.732\times10^{-4}$ | $-3.254\times10^{-3}$ | 0.949 | 0.3549 |
| $P\tau_{rot}$, RVT, HH PES | $-4.399\times10^{-4}$ | $2.823\times10^{-3}$ | 0.776 | $7.223\times10^{-2}$ |
| $P\tau_{vib}$, VT, HH PES | $-4.407\times10^{-6}$ | $-5.662\times10^{-3}$ | 0.5433 | $8.702\times10^{-2}$ |
| $P\tau_{vib}$, VT, Varandas and Pais PES [13] | $2.304\times10^{-3}$ | $-7.254\times10^{-2}$ | 1.245 | 1.7 |

where $P$ is the pressure; $P_{10}$ is the probability of vibrational deactivation; $\sigma_0$ is the gas-kinetic effective cross section; and $\mu$ and $\theta$ are the reduced mass of colliding particles and characteristic vibrational temperature of the target molecule, respectively. The vibrational relaxation time, given by Eq. (23), asymptotically converges to the MW equation at low temperatures, since $P_{10} \sim \exp(-T^{-1/3})$, as shown in [15]. Equation (23), known as the Landau–Teller equation, was derived under three assumptions: 1) The transitions occur only between the neighboring states. 2) The rate of transition is proportional to the vibrational quantum number.3) The states are populated according to the Boltzmann distribution. At higher temperatures, the vibrational relaxation deviates from that given by Eq. (23) due to the breakdown of the assumptions in the Landau–Teller theory.

Equation (23) was used in [15] to derive the $O_2$–$O_2$ and $O_2$–O relaxation times. The agreement between results in [15] and those generated by the present VT model is very satisfactory, and both results are substantially different from the MW relation. The relaxation times, calculated from the $K_{1\to0}$ rate in the present work and in [5], are in good agreement as well.

The vibrational and rotational relaxation times calculated by the e-folding method can be fit by a polynomial function of translational temperature in the range from 1000 to 20,000 K. The following function is used to approximate the relaxation times:

$$P\tau_x = 10^{-8}\left[A\left(\frac{T}{1000}\right)^3 + B\left(\frac{T}{1000}\right)^2 + C\left(\frac{T}{1000}\right) + D\right]$$

where $x$ stands for either the vibrational or rotational mode, $P\tau_x$ is in measurements of atmosphere $x$ second, and $T$ is in Kelvins. Coefficients $A$, $B$, $C$, and $D$ are given in Table 1. The root-mean-square error of the curve fit is not larger than $1.5\times10^{-3}\%$.

The relaxation time, obtained by means of the RVT model on the HH PES, is used to verify the adequacy of the Landau–Teller model, given by Eq. (21). The evolution of average vibrational and rotational energies, calculated from Eq. (21) using the relaxation parameters from Table 1, is compared to $\bar{e}_{vib}$ and $\bar{e}_{rot}$ obtained from Eqs. (15) and (16) in Figs. 7a and 7b. Chemical reactions are not considered. The pressure is set to 1.3625 atm at a heat bath temperature of 10,000 K. The Landau–Teller model perfectly describes the average energy of the rovibrational ladder at kinetic temperatures ranging from 1000 to 20,000 K using the relaxation times derived in the present work.

To make the results applicable in computational fluid dynamics codes, the state-resolved $O_2$–O VT transition rates based on the accurate Varandas and Pais PES [13] are curve fitted in the range of translation temperature from 1000 to 20,000 K. Transrotational equilibrium is assumed when averaging the QCT data over initial $j$. In the present work, the following function is used to describe the rates of vibrational deactivation:

$$K(T, v\to v') = 10^{-12}\exp\left(a_1 + \frac{a_2}{\log(T)} + a_3\log(T)\right) \qquad (24)$$

where $v \geq v'$, $T$ is in Kelvins; the transition rate $K(T, v\to v')$ is in cubic centimeters per second; and coefficients $a_1$, $a_2$, and $a_3$ for each of the 1128 transitions are specified in the Appendix. The present data have some important advantages over the results presented in [11]. The lower range of translational temperature is limited to 1000 K. At lower temperatures, the $O_2$–O transition rates vary drastically due to the large influence of the $O_3$ potential well, introducing larger errors in the curve fit. Thus, the present curve fit coefficients have smaller

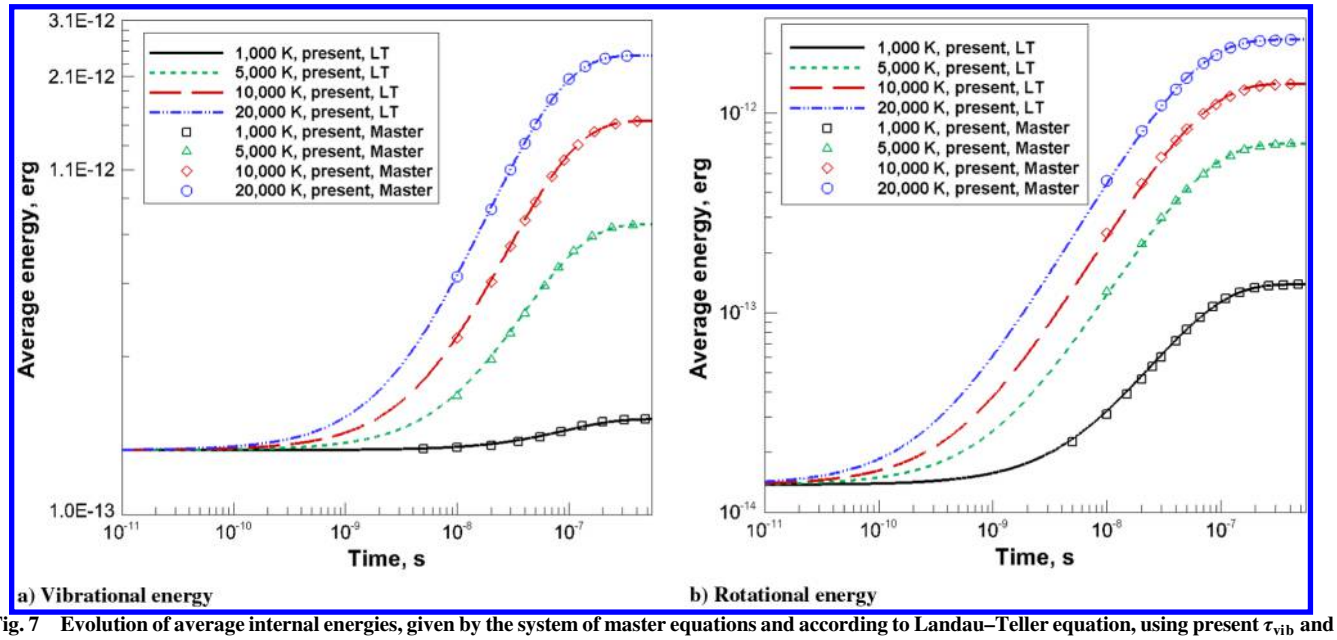


**Fig. 7 Evolution of average internal energies, given by the system of master equations and according to Landau–Teller equation, using present $\tau_{vib}$ and $\tau_{rot}$ relaxation times, derived from the HH PES.**

errors compared to those in [11]. The maximum error is 15% for $v = 41 - 46$ and is less than 6% for the rest. Additionally, the present rates are more accurate at temperatures above 10,000 K, since $O_2$–O collisions are simulated up to the kinetic energy of 6.5 eV. The data, given in Table A1, are available upon request.

### C. Analysis of RT and VT Rates

One can evaluate the rate of rotational-translational and vibrational-translational energy exchange using only the full set of rovibrational transition rates without involving the solution of master equations. The rate of total energy loss from vibrational level $v$ during the bound–bound transition to level $v_f$ can be expressed as follows [45]:

$$R_{v\to v'} = \frac{\sum_j e_{v,j}(2j+1)\exp(-(e_{v,j}-e_{v,0})/k_B T_{\rm rot})\sum_{j'} K(T,v,j\to v',j')}{\sum_j e_{v,j}(2j+1)\exp(-(e_{v,j}-e_{v,0})/k_B T_{\rm rot})} \tag{25}$$

It is assumed in Eq. (25) that the population of rotational levels is described by the Boltzmann distribution at temperature $T_{\rm rot}$. The similar expression for the energy gain by vibrational level $v'$ during the bound–bound transition from the level $v$ can be written as follows:

$$R_{v'\leftarrow v} = \frac{\sum_j (2j+1)\exp(-(e_{v,j}-e_{v,0})/k_B T_{\rm rot})\sum_{j'} e_{v',j'} K(T,v,j\to v',j')}{\sum_j e_{v,j}(2j+1)\exp(-(e_{v,j}-e_{v,0})/k_B T_{\rm rot})} \tag{26}$$

The loss and gain of energy, described by Eqs. (25) and (26), consist of vibrational and rotational contributions. To evaluate individual contributions, the vibrational energy of molecules in the ground rotational state must be subtracted:

$$R^{\rm rot}_{v\to v'} = R_{v\to v'} - R^{\rm vib}_{v\to v'} \tag{27}$$

$$R^{\rm rot}_{v'\leftarrow v} = R_{v'\leftarrow v} - R^{\rm vib}_{v'\leftarrow v} \tag{28}$$

where $R^{\rm vib}_{v\to v'} = e_{v,0}K(T,T_{\rm rot},v\to v')$ and $R^{\rm vib}_{v'\leftarrow v} = e_{v',0}K(T,T_{\rm rot},v'\to v)$ are the loss and gain of vibrational energy by state $v$. The gain and loss of rotational energy due to the bound–bound transitions between $v$ and $v'$ vibrational levels are given by Eqs. (27) and (28). The difference between

$$R^{\rm rot}_{v\to v'}$$

and

$$R^{\rm rot}_{v'\leftarrow v}$$

is due to the energy exchange between the rotational and translational degrees of freedom:

$$R^{T,{\rm rot}}_{v,v'} = R^{\rm rot}_{v\to v'} - R^{\rm rot}_{v'\leftarrow v} \tag{29}$$

A similar exchange term can be derived for the transvibrational energy exchange

$$R^{T,{\rm vib}}_{v,v'} = R^{\rm vib}_{v\to v'} - R^{\rm vib}_{v'\leftarrow v} \tag{30}$$

Note that $R^{\rm rot}_{v\to v'}$, $R^{\rm vib}_{v\to v'}$, $R^{\rm rot}_{v'\leftarrow v}$, and $R^{\rm vib}_{v'\leftarrow v}$ are positive, whereas $R^{T,{\rm rot}}_{v,v'}$ and $R^{T,{\rm vib}}_{v,v'}$ can be either positive or negative. Under shock conditions, when $T \gg T_r$, $T_v$, $R^{T,{\rm rot}}_{v,v'}$ and $R^{T,{\rm vib}}_{v,v'}$ are always positive, whereas in expanding flow, they can be negative. Equations (25–29) allow an investigation of the internal energy exchange in a relatively simple manner.

In the present work, the total rate of energy gain by internal modes is estimated using the transition rates from the HH PES. It is interesting to compare $R^{T,{\rm rot}}$ and $R^{T,{\rm vib}}$ in $O_2$–O collisions to that of another atom–molecule system. Colonna et al. [45] performed similar calculations for the collisions of the hydrogen molecule with its parent atom. The $O_2$–Ar state-resolved rates also became available recently [10]. In the present work, a comparison of rotational and vibrational energy gains is performed for the fixed internal temperature $T_{\rm rot} = T_{\rm vib} = 50$ K and translational temperature from $10^2$ to $10^5$ K. These parameters correspond to the typical conditions observed immediately behind a shock front.

$R^{T,{\rm rot}}$ and $R^{T,{\rm vib}}$ coefficients for the $O_2$–O, $H_2$–H, and $O_2$–Ar systems are shown in Fig. 8. These results do not indicate which species proceeds to equilibrium faster than the others, since all rates are normalized to their own maximum values. The energy gain by the translational mode (not shown in Fig. 8) is always negative, and the corresponding rate asymptotically approaches unity for all translational temperatures. This represents the loss of energy by

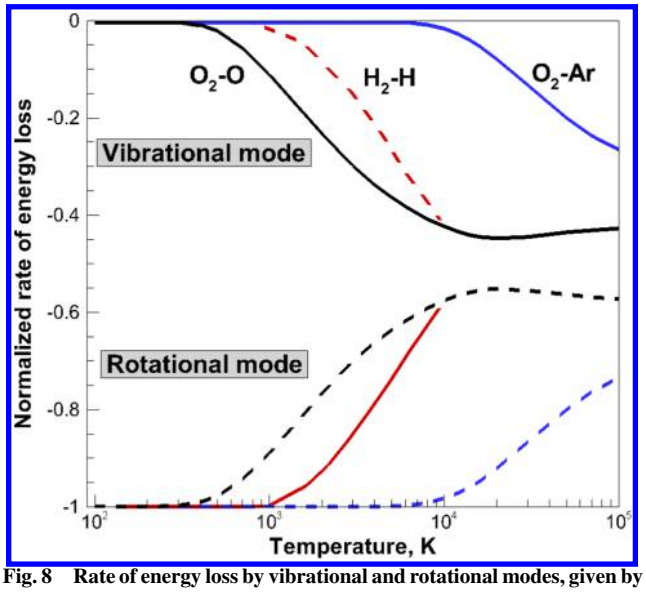


**Fig. 8 Rate of energy loss by vibrational and rotational modes, given by the HH PES.**

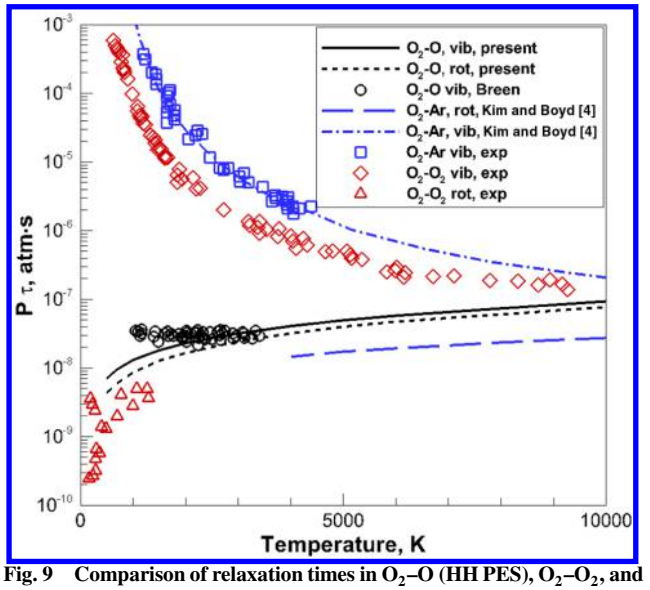


**Fig. 9 Comparison of relaxation times in $O_2$–O (HH PES), $O_2$–$O_2$, and $O_2$–Ar collisions (rot = rotational, vib = vibrational, and exp = experimental).**

translational degree of freedom. The negative sign of $R^{\text{rot}}$ and $R^{T,\text{vib}}$ corresponds to the gain of energy. At low temperatures, nearly all energy from the translational mode is spent to excite the rotational degrees of freedom, whereas the vibrational mode remains virtually inactive. This regime is observed at temperatures below 8000 K for $O_2$–Ar, 1000 K for hydrogen, and 400 K for $O_2$–O. As the temperature increases further, the energy from translational motion is shared between the vibrational and rotational degrees of freedom. Note that the rate of energy gain by the rotational mode is always larger than that by the vibrational mode.

Recent master equation studies of state-to-state kinetics of hydrogen [7] revealed a significant transrotational nonequilibrium at kinetic temperatures of 6000 K and higher. The presence of nonequilibrium can be judged by a relatively large deposition of kinetic energy into the vibrational degrees of freedom, compared to the rotational mode, as follows from Fig. 8. The same ratio of $R^{T,\text{rot}}$ and $R^{T,\text{vib}}$ for $O_2$–O collisions is observed at temperatures as low as 2000 K. Comparing $R^{T,\text{rot}}$ and $R^{T,\text{vib}}$ for $O_2$–Ar collisions, one may conclude that the rotational nonequilibrium in this case occurs at higher temperatures than in $O_2$–O and $H_2$–H collisions. The solution of master equations, performed in [10], indicates that the rate of rotational relaxation becomes important at kinetic temperatures of 10,000 K and higher. This result is in agreement with the expectation of rotational nonequilibrium in $H_2$–H and $O_2$–O collisions.

It is interesting to compare the vibrational and rotational relaxation times in $O_2$–O collisions with the relaxation times in pure oxygen, as well as in $O_2$ diluted by a chemically inactive gas, such as argon. An extensive overview of the experimental data on rotational relaxation in pure oxygen at temperatures below 1500 K can be found in [46]. To the authors' knowledge, the experimental data on $O_2$ rotational relaxation at higher temperatures do not exist. However, the rotational relaxation time in $O_2$–Ar collisions was recently calculated by the QCT method over a wide temperature range [10]. The $O_2$–O, $O_2$–Ar, and $O_2$–O relaxation times are shown in Fig. 9. Diamond and delta symbols correspond to the vibrational and rotational relaxation times in pure oxygen, taken from [40] and [46]. Square symbols correspond to the $O_2$–Ar vibrational relaxation time, measured in shock tube facilities [47]. Solid and short-dashed curves correspond to the vibrational and rotational relaxation times of $O_2$–O obtained in the present work by means of the RVT model via the HH PES. Long-dashed and dashed–dotted lines describe the rotational and vibrational relaxation in $O_2$–Ar [10].

It follows from Fig. 9 that the rotational nonequilibrium in $O_2$–Ar collisions is significant only at temperatures of 10,000 K and higher. Below these temperatures, the rotational relaxation time is two to three orders of magnitude smaller than the vibrational relaxation time. This fact confirms the conclusion drawn from Fig. 8. The $O_2$–$O_2$ and $O_2$–Ar vibrational relaxation times are nearly the same order of magnitude for the entire temperature range, indicating that the mechanisms of transvibrational energy exchange in these systems are similar.

The experimental data on rotational relaxation in pure oxygen are ambiguous and are limited to temperatures from 150 to 1200 K. The rotational relaxation in $O_2$–O proceeds more slowly than in pure oxygen at these temperatures. On the contrary, the $O_2$–O vibrational relaxation time is more than three orders of magnitude smaller than that in $O_2$–$O_2$ collisions. Moreover, one can notice the opposite slopes of vibrational relaxation times for the $O_2$–$O_2$, $O_2$–Ar, and $O_2$–O collisions. The explanation of this phenomenon lies in the different mechanisms of vibrational relaxation for the considered species.

### D. Nonreactive and Exchange Channels of Reaction

The exchange channel in collisions of oxygen with the parent atom has a significant impact on the process of internal energy transfer. Bauer and Tsang [41] have made an assumption that the vibrational relaxation in the $O_3$ complex occurs entirely via the exchange channel. This observation was partially confirmed by Esposito and Capitelli [11]. They demonstrated the importance of the exchange channel by comparing rates of removal and monoquantum deactivation from the first excited vibrational level. The exchange mechanism contributes up to 30% to the total rate of monoquantum deactivation at temperatures below 300 K, rapidly diminishing at high temperatures. Particular interest in the exchange reaction is due to its absence in collisions of oxygen with other species, such as argon. The present paper analyzes the contribution of the exchange reaction to the vibrational relaxation in a straightforward manner by computing the corresponding transition probability over a wide range of collision energies.

Vibrational transition probabilities via the exchange and nonreactive channels in $O_2$–O and $O_2$–Ar collisions are shown in Figs. 10a and 10b, respectively, for the initial state ($v = 1$, $j = 1$). For $O_2$–O, probabilities are obtained from the Varandas and Pais PES [13]. Details on $O_2$–Ar calculations are given in [10]. Solid and dashed curves correspond to the exchange and nonreactive channels, respectively. The probability of vibrationally elastic transition is shown for reference by curves with symbols. One can see that vibrational transitions in $O_2$–O collisions occur at much lower kinetic energies than in the $O_2$–Ar interaction. In the latter case, the QCT method resolves only rotational transitions at collision energies lower than 1.7 eV. This fact explains an efficient rotational relaxation compared to the vibrational mode in the $O_2$–Ar mixture. Here, one

should note that the number of trajectories, adopted for the $O_2$–Ar QCT simulation, was 2000. The vibrational transition probability for these species at low temperatures is orders of magnitude smaller than that in $O_2$–O collisions, as follows from Fig. 9. Thus, to obtain accurate vibrational transition probabilities for the $O_2$–Ar system, one should significantly increase the number of trajectories in the QCT simulation. At the same time, the probability of vibrational deactivation is comparable for the $O_2$–O and $O_2$–Ar systems at energies above 5 eV, which explains the close vibrational relaxation times in Fig. 5.

The exchange and nonreactive channels of deactivation are both active in $O_2$–O collisions starting from very low energy. The contribution of the exchange channel is significant for energies below 1 eV; however, at higher energies, the exchange probability rapidly approaches to zero. The exchange probability during the vibrationally elastic collision is small for all considered energies.

The vibrational energy randomization is also studied for high-lying levels in Figs. 11a and 11b for the initial state $v_i = 20$, $j = 1$. The probability of multiquantum vibrational deactivation at low collision energies is strongly dependent on the exchange channel. The latter contribution is nearly twice as high as the probability of the nonreactive channel at kinetic energies between 0.1 and 1 eV. The contribution of the exchange channel diminishes at high energies, whereas the nonreactive channel remains open. This situation also takes place in transitions to higher vibrational states, as shown in Fig. 11b. More important, the exchange plays a dominant role in large multiquantum jumps rather than in transitions with small energy randomization, as follows from Fig. 11a. For the transition $v = 20 \rightarrow v' = 15$, the nonreactive channel plays a major role for energies of 1 eV and higher, whereas for the transition $v = 20 \rightarrow v' = 0$, this takes place only at energies higher than 10 eV.

## V. Conclusions

Two sets of transition rates in $O_2$–O collisions are generated by means of the QCT method for each vibrational state using the

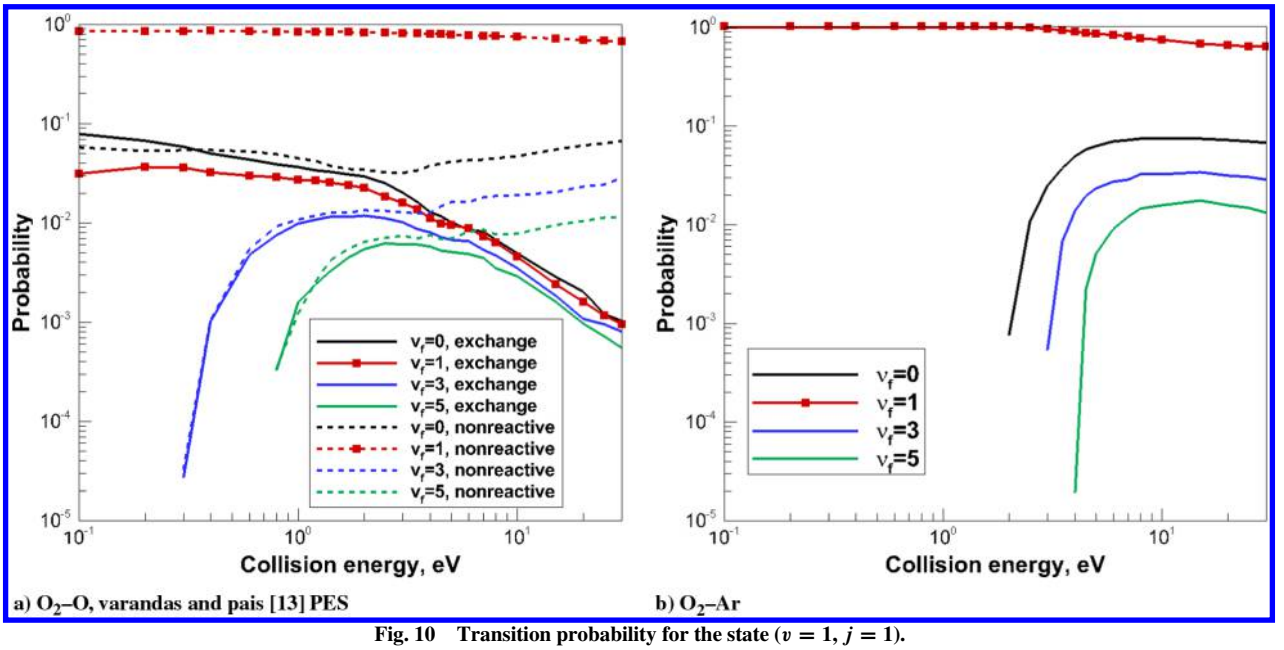


**Fig. 10 Transition probability for the state ($v = 1$, $j = 1$).**

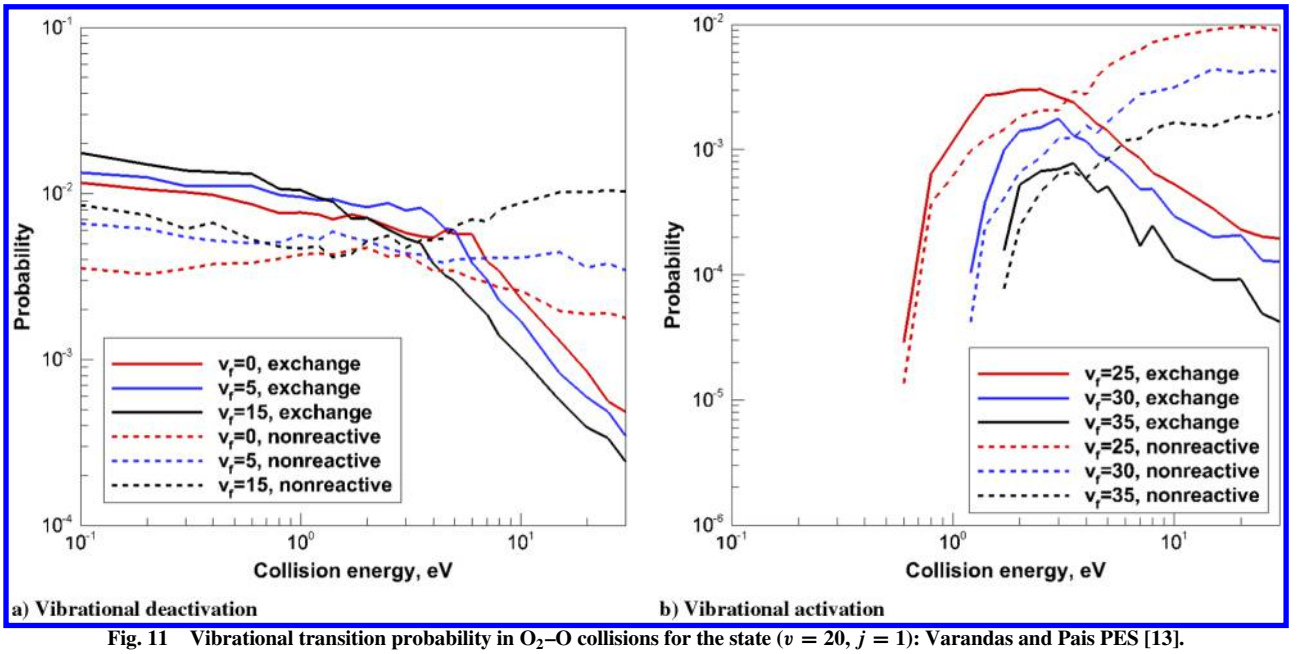


**Fig. 11 Vibrational transition probability in $O_2$–O collisions for the state ($v = 20$, $j = 1$): Varandas and Pais PES [13].**

Varandas and Pais PES [13] and for each rovibrational state using the PES obtained from the Hulburt–Hirschfelder potential. These PESs are different by the presence of the $O_3$ three-body interaction term. The vibrational and rotational relaxations of oxygen in collisions with its parent atom are modeled by the master equation, constructed for each vibrational and rovibrational state. A heat bath of oxygen at a constant temperature between 1000 and 20,000 K is considered under the assumption of transrotational equilibrium (VT model), as well as treating rotational and vibrational relaxation in a similar manner (RVT model).

The present VT and RVT models satisfactorily reproduce the experimental data on $O_2$–O vibrational relaxation time in the range of experimental measurements between 1000 and 3600 K. However, the relaxation time, derived from the solution of master equations, has a significantly different temperature dependence compared to that in the conventional Millikan–White equation. Namely, the vibrational relaxation in $O_2$–O collisions is very effective at low temperatures, and it slowly increases toward the high–temperature limit. The rotational and vibrational relaxation times are comparable in the range of temperature between 1000 and 10,000 K, suggesting that the vibrational and rotational modes should be treated individually.

Trajectory simulations, carried out on the Varandas and Pais [13] and HH PESs, revealed a similar temperature dependence of vibrational relaxation times. The former PES predicts slower vibrational relaxation compared to that of the HH PES. The difference in relaxation times between the Varandas and Pais [13] and HH PESs increases at low temperatures, indicating the importance of the geometry and depth of the $O_3$ potential well at these conditions. At high temperatures, the difference in transition rates between these two PESs becomes small due to the predominant interaction of the target and projectile via the repulsive branches of the potential. It is of interest to investigate the dynamics of $O_2$–O collisions on completely ab initio PES in the future, as well as to expand the range of existing experimental measurements.

In the present work, convenient relations for the e-fold rotational and vibrational relaxation times are derived. The Landau–Teller model accurately describes the evolution of the average vibrational and rotational energies using the present relaxation parameters. The detailed analysis of the state-to-state transition rates indicates that rotational nonequilibrium in $O_2$–O collisions occurs at much lower temperatures than in $H_2$–H and $O_2$–Ar mixtures. This fact may be important when modeling shock flows with a significant amount of oxygen atoms.

The probabilities of $O_2$–O multi- and monoquantum vibrational jumps are comparable with each other. This result is profoundly different from what is typically observed in molecular systems with a large repulsive potential. Meanwhile, the exchange channel of the $O_2$–O collision has a large impact on the internal energy randomization. The probability of the exchange trajectory that leads to a vibrational deactivation is larger than that of the nonreactive channel at low collision energies. The contribution of the exchange channel diminishes with collision energy, and vibrational deactivation at high temperatures occurs mostly via inelastic collisions. The contribution of the exchange channel to the process of energy randomization is more significant for large vibrational jumps. A database of vibrational transition rates, computed on the Varandas and Pais PES [13] assuming transrotational equilibrium is given in the Appendix for temperatures between 1000 and 20,000 K.

## Appendix: Curve Fit Coefficients of VT Transition Rates

See Table A1.

**Table A1 Curve fit coefficients of VT transitions rates**

| $\nu_i$ | $\nu_f$ | $a1$ | $a2$ | $a3$ |
|---|---|---|---|---|
| 1 | 1 | 6.141 − 1 | 2.522 + 0 | 3.968 − 1 |
| 1 | 0 | 1.471 − 1 | −7.504 − 1 | 2.214 − 1 |
| 2 | 2 | 1.248 + 0 | −2.005 − 1 | 3.563 − 1 |
| 2 | 1 | −3.765 + 0 | 1.029 + 1 | 4.990 − 1 |
| 2 | 0 | 4.723 + 0 | −1.883 + 1 | −1.070 − 1 |
| 3 | 3 | 8.763 − 1 | 1.060 + 0 | 3.785 − 1 |
| 3 | 2 | −5.033 + 0 | 1.206 + 1 | 6.066 − 1 |
| 3 | 1 | 2.402 + 0 | −1.144 + 1 | 4.142 − 2 |
| 3 | 0 | 5.858 + 0 | −2.473 + 1 | −1.846 − 1 |
| 4 | 4 | 3.073 − 1 | 3.551 + 0 | 4.079 − 1 |
| 4 | 3 | −6.546 + 0 | 1.593 + 1 | 7.174 − 1 |
| 4 | 2 | 4.456 − 1 | −5.513 + 0 | 1.718 − 1 |
| 4 | 1 | 4.552 + 0 | −2.006 + 1 | −1.115 − 1 |
| 4 | 0 | 6.926 + 0 | −3.023 + 1 | −2.528 − 1 |
| 5 | 5 | 2.040 + 0 | −3.822 + 0 | 3.053 − 1 |
| 5 | 4 | −6.987 + 0 | 1.610 + 1 | 7.584 − 1 |
| 5 | 3 | −1.481 + 0 | 4.622 − 1 | 3.017 − 1 |
| 5 | 2 | 3.359 + 0 | −1.654 + 1 | −3.504 − 2 |
| 5 | 1 | 5.830 + 0 | −2.580 + 1 | −1.984 − 1 |
| 5 | 0 | 7.029 + 0 | −3.134 + 1 | −2.644 − 1 |
| 6 | 6 | 1.606 − 1 | 3.858 + 0 | 4.175 − 1 |
| 6 | 5 | −8.538 + 0 | 2.148 + 1 | 8.585 − 1 |
| 6 | 4 | −3.085 + 0 | 5.989 + 0 | 4.036 − 1 |
| 6 | 3 | 1.376 + 0 | −9.496 + 0 | 8.721 − 2 |
| 6 | 2 | 4.241 + 0 | −2.008 + 1 | −1.038 − 1 |
| 6 | 1 | 5.006 + 0 | −2.296 + 1 | −1.551 − 1 |
| 6 | 0 | 7.354 + 0 | −3.297 + 1 | −2.919 − 1 |
| 7 | 7 | −3.333 + 0 | 1.705 + 1 | 6.440 − 1 |
| 7 | 6 | −8.792 + 0 | 2.168 + 1 | 8.806 − 1 |
| 7 | 5 | −4.002 + 0 | 8.597 + 0 | 4.660 − 1 |
| 7 | 4 | −1.188 − 1 | −4.374 + 0 | 1.815 − 1 |
| 7 | 3 | 3.090 + 0 | −1.630 + 1 | −3.210 − 2 |
| 7 | 2 | 4.372 + 0 | −2.105 + 1 | −1.181 − 1 |
| 7 | 1 | 5.711 + 0 | −2.633 + 1 | −2.027 − 1 |
| 7 | 0 | 7.121 + 0 | −3.208 + 1 | −2.868 − 1 |
| 8 | 8 | −2.679 + 1 | 1.080 + 2 | 2.142 + 0 |
| 8 | 7 | −1.029 + 1 | 2.745 + 1 | 9.725 − 1 |
| 8 | 6 | −4.672 + 0 | 1.059 + 1 | 5.108 − 1 |
| 8 | 5 | −6.407 − 1 | −3.038 + 0 | 2.168 − 1 |
| 8 | 4 | 1.557 + 0 | −1.070 + 1 | 6.096 − 2 |
| 8 | 3 | 4.056 + 0 | −2.049 + 1 | −9.898 − 2 |
| 8 | 2 | 5.158 + 0 | −2.485 + 1 | −1.683 − 1 |
| 8 | 1 | 5.544 + 0 | −2.614 + 1 | −1.952 − 1 |
| 8 | 0 | 6.833 + 0 | −3.110 + 1 | −2.768 − 1 |
| 9 | 9 | 8.638 − 1 | 6.890 − 1 | 3.730 − 1 |
| 9 | 8 | −1.129 + 1 | 3.157 + 1 | 1.030 + 0 |
| 9 | 7 | −5.791 + 0 | 1.501 + 1 | 5.757 − 1 |
| 9 | 6 | −5.600 − 1 | −3.944 + 0 | 2.148 − 1 |
| 9 | 5 | 1.343 + 0 | −1.031 + 1 | 7.494 − 2 |
| 9 | 4 | 2.804 + 0 | −1.590 + 1 | −2.237 − 2 |
| 9 | 3 | 3.729 + 0 | −1.959 + 1 | −8.213 − 2 |
| 9 | 2 | 5.271 + 0 | −2.583 + 1 | −1.772 − 1 |
| 9 | 1 | 5.501 + 0 | −2.638 + 1 | −1.960 − 1 |
| 9 | 0 | 5.478 + 0 | −2.590 + 1 | −1.992 − 1 |
| 10 | 10 | 1.646 + 0 | −2.714 + 0 | 3.266 − 1 |
| 10 | 9 | −1.230 + 1 | 3.529 + 1 | 1.093 + 0 |
| 10 | 8 | −7.232 + 0 | 2.131 + 1 | 6.547 − 1 |
| 10 | 7 | −1.530 + 0 | 2.578 − 1 | 2.673 − 1 |
| 10 | 6 | 1.005 + 0 | −9.025 + 0 | 9.223 − 2 |
| 10 | 5 | 2.400 + 0 | −1.452 + 1 | 7.363 − 4 |
| 10 | 4 | 4.066 + 0 | −2.118 + 1 | −1.044 − 1 |
| 10 | 3 | 4.660 + 0 | −2.377 + 1 | −1.409 − 1 |
| 10 | 2 | 4.784 + 0 | −2.439 + 1 | −1.479 − 1 |
| 10 | 1 | 5.097 + 0 | −2.530 + 1 | −1.733 − 1 |
| 10 | 0 | 5.081 + 0 | −2.517 + 1 | −1.727 − 1 |
| 11 | 11 | 8.000 − 1 | 6.424 − 1 | 3.774 − 1 |
| 11 | 10 | −1.189 + 1 | 3.248 + 1 | 1.080 + 0 |
| 11 | 9 | −8.767 + 0 | 2.769 + 1 | 7.420 − 1 |
| 11 | 8 | −2.963 + 0 | 6.811 + 0 | 3.418 − 1 |
| 11 | 7 | 4.523 − 1 | −6.499 + 0 | 1.200 − 1 |
| 11 | 6 | 3.540 + 0 | −1.917 + 1 | −7.100 − 2 |
| 11 | 5 | 3.533 + 0 | −1.908 + 1 | −7.548 − 2 |
| 11 | 4 | 4.993 + 0 | −2.519 + 1 | −1.648 − 1 |
| 11 | 3 | 5.149 + 0 | −2.602 + 1 | −1.733 − 1 |

## Acknowledgments

The authors gratefully acknowledge funding for this work through U.S. Air Force Office of Scientific Research grant FA9550-12-1-0483. D. Andrienko would like to thank Jae Gang Kim for the $O_2 - Ar$ quasi-classical trajectory program code and numerous fruitful discussions, as well as Kevin Neitzel for the curve fitting tool.

**Table A1** (*Continued.*)

| $\nu_i$ | $\nu_f$ | $a1$ | $a2$ | $a3$ |
|---|---|---|---|---|
| 11 | 2 | 4.964 + 0 | −2.540 + 1 | −1.622 − 1 |
| 11 | 1 | 4.141 + 0 | −2.218 + 1 | −1.127 − 1 |
| 11 | 0 | 4.752 + 0 | −2.479 + 1 | −1.503 − 1 |
| 12 | 12 | 1.321 + 0 | −1.763 + 0 | 3.481 − 1 |
| 12 | 11 | −1.118 + 1 | 2.844 + 1 | 1.048 + 0 |
| 12 | 10 | −8.839 + 0 | 2.706 + 1 | 7.537 − 1 |
| 12 | 9 | −5.148 + 0 | 1.616 + 1 | 4.641 − 1 |
| 12 | 8 | −8.920 − 1 | −2.272 − 2 | 1.856 − 1 |
| 12 | 7 | 2.666 + 0 | −1.498 + 1 | −2.901 − 2 |
| 12 | 6 | 4.304 + 0 | −2.210 + 1 | −1.257 − 1 |
| 12 | 5 | 4.395 + 0 | −2.267 + 1 | −1.323 − 1 |
| 12 | 4 | 4.555 + 0 | −2.351 + 1 | −1.422 − 1 |
| 12 | 3 | 4.812 + 0 | −2.483 + 1 | −1.570 − 1 |
| 12 | 2 | 4.151 + 0 | −2.224 + 1 | −1.182 − 1 |
| 12 | 1 | 5.326 + 0 | −2.789 + 1 | −1.804 − 1 |
| 12 | 0 | 5.248 + 0 | −2.822 + 1 | −1.707 − 1 |
| 13 | 13 | 1.005 + 0 | −3.411 − 1 | 3.637 − 1 |
| 13 | 12 | −1.093 + 1 | 2.695 + 1 | 1.038 + 0 |
| 13 | 11 | −1.030 + 1 | 3.201 + 1 | 8.509 − 1 |
| 13 | 10 | −5.100 + 0 | 1.517 + 1 | 4.667 − 1 |
| 13 | 9 | −1.740 + 0 | 3.945 + 0 | 2.270 − 1 |
| 13 | 8 | 1.644 + 0 | −1.006 + 1 | 2.146 − 2 |
| 13 | 7 | 4.847 + 0 | −2.380 + 1 | −1.674 − 1 |
| 13 | 6 | 4.474 + 0 | −2.254 + 1 | −1.453 − 1 |
| 13 | 5 | 4.277 + 0 | −2.195 + 1 | −1.334 − 1 |
| 13 | 4 | 3.584 + 0 | −1.947 + 1 | −9.070 − 2 |
| 13 | 3 | 4.206 + 0 | −2.245 + 1 | −1.255 − 1 |
| 13 | 2 | 4.665 + 0 | −2.524 + 1 | −1.438 − 1 |
| 13 | 1 | 5.241 + 0 | −2.860 + 1 | −1.683 − 1 |
| 13 | 0 | 5.515 + 0 | −3.092 + 1 | −1.739 − 1 |
| 14 | 14 | 2.100 + 0 | −4.803 + 0 | 2.963 − 1 |
| 14 | 13 | −1.114 + 1 | 2.747 + 1 | 1.052 + 0 |
| 14 | 12 | −1.079 + 1 | 3.329 + 1 | 8.866 − 1 |
| 14 | 11 | −4.856 + 0 | 1.307 + 1 | 4.618 − 1 |
| 14 | 10 | −1.966 + 0 | 4.057 + 0 | 2.461 − 1 |
| 14 | 9 | 6.758 − 1 | −5.724 + 0 | 7.220 − 2 |
| 14 | 8 | 2.944 + 0 | −1.507 + 1 | −6.656 − 2 |
| 14 | 7 | 5.259 + 0 | −2.535 + 1 | −1.994 − 1 |
| 14 | 6 | 4.326 + 0 | −2.168 + 1 | −1.449 − 1 |
| 14 | 5 | 3.028 + 0 | −1.716 + 1 | −5.945 − 2 |
| 14 | 4 | 2.800 + 0 | −1.666 + 1 | −4.376 − 2 |
| 14 | 3 | 3.341 + 0 | −1.943 + 1 | −7.236 − 2 |
| 14 | 2 | 5.201 + 0 | −2.807 + 1 | −1.743 − 1 |
| 14 | 1 | 5.459 + 0 | −3.032 + 1 | −1.792 − 1 |
| 14 | 0 | 6.471 + 0 | −3.565 + 1 | −2.285 − 1 |
| 15 | 15 | 5.746 − 1 | 1.279 + 0 | 3.883 − 1 |
| 15 | 14 | −1.215 + 1 | 3.175 + 1 | 1.110 + 0 |
| 15 | 13 | −1.187 + 1 | 3.758 + 1 | 9.497 − 1 |
| 15 | 12 | −7.316 + 0 | 2.290 + 1 | 6.084 − 1 |
| 15 | 11 | −3.364 + 0 | 8.979 + 0 | 3.365 − 1 |
| 15 | 10 | −7.706 − 1 | −2.409 − 2 | 1.569 − 1 |
| 15 | 9 | 1.795 + 0 | −9.572 + 0 | −1.053 − 2 |
| 15 | 8 | 3.165 + 0 | −1.546 + 1 | −9.020 − 2 |
| 15 | 7 | 3.559 + 0 | −1.793 + 1 | −1.072 − 1 |
| 15 | 6 | 2.293 + 0 | −1.334 + 1 | −2.791 − 2 |
| 15 | 5 | 1.812 + 0 | −1.225 + 1 | 7.808 − 3 |
| 15 | 4 | 2.722 + 0 | −1.696 + 1 | −3.670 − 2 |
| 15 | 3 | 3.361 + 0 | −1.990 + 1 | −7.429 − 2 |
| 15 | 2 | 3.832 + 0 | −2.298 + 1 | −9.129 − 2 |
| 15 | 1 | 5.241 + 0 | −3.038 + 1 | −1.590 − 1 |
| 15 | 0 | 5.814 + 0 | −3.351 + 1 | −1.885 − 1 |
| 16 | 16 | 7.934 − 1 | 3.250 − 1 | 3.749 − 1 |
| 16 | 15 | −1.380 + 1 | 3.859 + 1 | 1.208 + 0 |
| 16 | 14 | −1.729 + 1 | 6.093 + 1 | 1.260 + 0 |
| 16 | 13 | −1.113 + 1 | 3.934 + 1 | 8.260 − 1 |
| 16 | 12 | −7.528 + 0 | 2.666 + 1 | 5.757 − 1 |
| 16 | 11 | −3.697 + 0 | 1.211 + 1 | 3.278 − 1 |
| 16 | 10 | −1.423 + 0 | 4.228 + 0 | 1.724 − 1 |
| 16 | 9 | −1.562 + 0 | 5.652 + 0 | 1.693 − 1 |
| 16 | 8 | −3.608 − 1 | 3.969 − 1 | 9.794 − 2 |
| 16 | 7 | 2.894 − 1 | −3.795 + 0 | 7.499 − 2 |
| 16 | 6 | −5.108 − 1 | −1.645 + 0 | 1.331 − 1 |
| 16 | 5 | −5.596 − 1 | −2.501 + 0 | 1.455 − 1 |
| 16 | 4 | −3.790 − 1 | −3.899 + 0 | 1.397 − 1 |
| 16 | 3 | 8.470 − 1 | −9.643 + 0 | 7.265 − 2 |

**Table A1** (*Continued.*)

| $\nu_i$ | $\nu_f$ | $a1$ | $a2$ | $a3$ |
|---|---|---|---|---|
| 16 | 2 | 2.507 + 0 | −1.772 + 1 | −1.478 − 2 |
| 16 | 1 | 3.241 + 0 | −2.210 + 1 | −4.600 − 2 |
| 16 | 0 | 5.090 + 0 | −3.056 + 1 | −1.499 − 1 |
| 17 | 17 | −1.420 − 1 | 3.987 + 0 | 4.315 − 1 |
| 17 | 16 | −1.261 + 1 | 3.266 + 1 | 1.147 + 0 |
| 17 | 15 | −1.503 + 1 | 5.056 + 1 | 1.135 + 0 |
| 17 | 14 | −1.250 + 1 | 4.470 + 1 | 9.089 − 1 |
| 17 | 13 | −8.699 + 0 | 3.148 + 1 | 6.427 − 1 |
| 17 | 12 | −4.481 + 0 | 1.534 + 1 | 3.709 − 1 |
| 17 | 11 | −2.260 + 0 | 6.983 + 0 | 2.269 − 1 |
| 17 | 10 | −1.148 + 0 | 3.554 + 0 | 1.458 − 1 |
| 17 | 9 | −1.394 + 0 | 5.412 + 0 | 1.490 − 1 |
| 17 | 8 | 4.067 − 3 | −1.295 + 0 | 7.441 − 2 |
| 17 | 7 | 9.268 − 1 | −6.960 + 0 | 3.885 − 2 |
| 17 | 6 | 7.361 − 2 | −4.568 + 0 | 9.981 − 2 |
| 17 | 5 | 4.416 − 1 | −7.033 + 0 | 8.555 − 2 |
| 17 | 4 | 7.658 − 1 | −9.197 + 0 | 7.395 − 2 |
| 17 | 3 | 1.611 + 0 | −1.346 + 1 | 3.054 − 2 |
| 17 | 2 | 2.124 + 0 | −1.633 + 1 | 4.988 − 3 |
| 17 | 1 | 2.508 + 0 | −1.918 + 1 | −4.826 − 3 |
| 17 | 0 | 3.423 + 0 | −2.378 + 1 | −5.447 − 2 |
| 18 | 18 | 1.623 − 1 | 2.637 + 0 | 4.132 − 1 |
| 18 | 17 | −1.197 + 1 | 2.966 + 1 | 1.112 + 0 |
| 18 | 16 | −1.522 + 1 | 5.028 + 1 | 1.157 + 0 |
| 18 | 15 | −1.183 + 1 | 4.086 + 1 | 8.792 − 1 |
| 18 | 14 | −8.286 + 0 | 2.922 + 1 | 6.218 − 1 |
| 18 | 13 | −4.973 + 0 | 1.735 + 1 | 3.984 − 1 |
| 18 | 12 | −2.727 + 0 | 9.017 + 0 | 2.509 − 1 |
| 18 | 11 | −1.049 + 0 | 3.069 + 0 | 1.376 − 1 |
| 18 | 10 | −2.085 − 2 | −6.660 − 1 | 6.977 − 2 |
| 18 | 9 | −5.626 − 1 | 1.867 + 0 | 9.650 − 2 |
| 18 | 8 | −2.127 − 1 | −1.012 + 0 | 9.053 − 2 |
| 18 | 7 | 2.782 − 1 | −4.909 + 0 | 8.095 − 2 |
| 18 | 6 | 1.158 + 0 | −9.546 + 0 | 3.659 − 2 |
| 18 | 5 | 9.747 − 2 | −6.242 + 0 | 1.108 − 1 |
| 18 | 4 | 3.891 − 1 | −8.184 + 0 | 9.830 − 2 |
| 18 | 3 | 1.219 + 0 | −1.228 + 1 | 5.383 − 2 |
| 18 | 2 | 9.080 − 1 | −1.157 + 1 | 7.665 − 2 |
| 18 | 1 | 7.519 − 1 | −1.169 + 1 | 9.152 − 2 |
| 18 | 0 | 2.931 + 0 | −2.137 + 1 | −3.330 − 2 |
| 19 | 19 | −5.005 − 2 | 3.468 + 0 | 4.250 − 1 |
| 19 | 18 | −1.102 + 1 | 2.549 + 1 | 1.058 + 0 |
| 19 | 17 | −1.580 + 1 | 5.240 + 1 | 1.193 + 0 |
| 19 | 16 | −1.252 + 1 | 4.303 + 1 | 9.253 − 1 |
| 19 | 15 | −8.433 + 0 | 2.913 + 1 | 6.339 − 1 |
| 19 | 14 | −5.236 + 0 | 1.750 + 1 | 4.217 − 1 |
| 19 | 13 | −3.550 + 0 | 1.227 + 1 | 2.986 − 1 |
| 19 | 12 | −1.964 + 0 | 6.934 + 0 | 1.876 − 1 |
| 19 | 11 | −1.100 + 0 | 3.614 + 0 | 1.330 − 1 |
| 19 | 10 | −1.185 + 0 | 4.005 + 0 | 1.369 − 1 |
| 19 | 9 | −6.953 − 1 | 1.786 + 0 | 1.088 − 1 |
| 19 | 8 | 5.894 − 1 | −4.963 + 0 | 4.699 − 2 |
| 19 | 7 | 1.743 + 0 | −1.131 + 1 | −6.184 − 3 |
| 19 | 6 | 1.166 + 0 | −1.051 + 1 | 4.437 − 2 |
| 19 | 5 | 7.955 − 1 | −9.422 + 0 | 6.720 − 2 |
| 19 | 4 | 9.143 − 1 | −1.049 + 1 | 6.383 − 2 |
| 19 | 3 | 4.881 − 1 | −9.459 + 0 | 9.590 − 2 |
| 19 | 2 | −6.616 − 2 | −7.624 + 0 | 1.302 − 1 |
| 19 | 1 | 9.546 − 1 | −1.260 + 1 | 7.637 − 2 |
| 19 | 0 | 7.531 − 1 | −1.215 + 1 | 8.907 − 2 |
| 20 | 20 | −5.633 − 1 | 5.219 + 0 | 4.591 − 1 |
| 20 | 19 | −1.098 + 1 | 2.502 + 1 | 1.059 + 0 |
| 20 | 18 | −1.521 + 1 | 4.940 + 1 | 1.162 + 0 |
| 20 | 17 | −1.239 + 1 | 4.198 + 1 | 9.203 − 1 |
| 20 | 16 | −8.241 + 0 | 2.739 + 1 | 6.317 − 1 |
| 20 | 15 | −5.497 + 0 | 1.777 + 1 | 4.429 − 1 |
| 20 | 14 | −3.261 + 0 | 1.049 + 1 | 2.843 − 1 |
| 20 | 13 | −2.594 + 0 | 8.942 + 0 | 2.300 − 1 |
| 20 | 12 | −1.520 + 0 | 5.498 + 0 | 1.526 − 1 |
| 20 | 11 | −1.832 + 0 | 6.523 + 0 | 1.742 − 1 |
| 20 | 10 | −8.574 − 1 | 2.556 + 0 | 1.145 − 1 |
| 20 | 9 | −4.627 − 1 | 4.657 − 1 | 9.529 − 2 |
| 20 | 8 | 5.117 − 1 | −5.050 + 0 | 5.345 − 2 |
| 20 | 7 | 1.071 + 0 | −8.966 + 0 | 3.567 − 2 |
| 20 | 6 | 1.469 + 0 | −1.168 + 1 | 2.069 − 2 |

**Table A1** (*Continued.*)

| $\nu_i$ | $\nu_f$ | $a1$ | $a2$ | $a3$ |
|---|---|---|---|---|
| 20 | 5 | 1.290 + 0 | −1.197 + 1 | 4.029 − 2 |
| 20 | 4 | 7.764 − 1 | −1.039 + 1 | 7.445 − 2 |
| 20 | 3 | 6.572 − 1 | −1.027 + 1 | 8.174 − 2 |
| 20 | 2 | 6.810 − 1 | −1.098 + 1 | 8.535 − 2 |
| 20 | 1 | 2.872 − 1 | −9.814 + 0 | 1.100 − 1 |
| 20 | 0 | 4.212 − 2 | −8.881 + 0 | 1.233 − 1 |
| 21 | 21 | −7.878 + 0 | 3.378 + 1 | 9.225 − 1 |
| 21 | 20 | −9.218 + 0 | 1.746 + 1 | 9.570 − 1 |
| 21 | 19 | −1.562 + 1 | 5.082 + 1 | 1.189 + 0 |
| 21 | 18 | −1.373 + 1 | 4.721 + 1 | 1.002 + 0 |
| 21 | 17 | −8.612 + 0 | 2.859 + 1 | 6.544 − 1 |
| 21 | 16 | −5.535 + 0 | 1.759 + 1 | 4.453 − 1 |
| 21 | 15 | −4.418 + 0 | 1.457 + 1 | 3.580 − 1 |
| 21 | 14 | −2.355 + 0 | 7.224 + 0 | 2.205 − 1 |
| 21 | 13 | −1.149 + 0 | 3.234 + 0 | 1.363 − 1 |
| 21 | 12 | −9.573 − 1 | 2.954 + 0 | 1.179 − 1 |
| 21 | 11 | −2.255 − 1 | −2.267 − 1 | 7.643 − 2 |
| 21 | 10 | −7.165 − 1 | 1.609 + 0 | 1.071 − 1 |
| 21 | 9 | 4.839 − 1 | −3.916 + 0 | 4.093 − 2 |
| 21 | 8 | 7.060 − 1 | −5.872 + 0 | 3.773 − 2 |
| 21 | 7 | 2.335 + 0 | −1.437 + 1 | −4.177 − 2 |
| 21 | 6 | 1.834 + 0 | −1.348 + 1 | −7.405 − 4 |
| 21 | 5 | 1.218 + 0 | −1.185 + 1 | 4.341 − 2 |
| 21 | 4 | −2.594 − 1 | −6.429 + 0 | 1.358 − 1 |
| 21 | 3 | 1.894 − 1 | −8.276 + 0 | 1.040 − 1 |
| 21 | 2 | −5.737 − 1 | −5.933 + 0 | 1.576 − 1 |
| 21 | 1 | −2.078 + 0 | 8.646 − 2 | 2.450 − 1 |
| 21 | 0 | −1.380 + 0 | −2.837 + 0 | 2.003 − 1 |
| 22 | 22 | −2.469 + 1 | 9.351 + 1 | 2.096 + 0 |
| 22 | 21 | −9.867 + 0 | 2.048 + 1 | 9.912 − 1 |
| 22 | 20 | −1.577 + 1 | 5.142 + 1 | 1.196 + 0 |
| 22 | 19 | −1.212 + 1 | 4.028 + 1 | 9.079 − 1 |
| 22 | 18 | −8.594 + 0 | 2.822 + 1 | 6.542 − 1 |
| 22 | 17 | −5.964 + 0 | 1.893 + 1 | 4.734 − 1 |
| 22 | 16 | −3.413 + 0 | 9.867 + 0 | 3.007 − 1 |
| 22 | 15 | −2.868 + 0 | 8.786 + 0 | 2.532 − 1 |
| 22 | 14 | −2.101 + 0 | 6.302 + 0 | 1.992 − 1 |
| 22 | 13 | −1.432 + 0 | 4.312 + 0 | 1.503 − 1 |
| 22 | 12 | −5.934 − 1 | 1.144 + 0 | 9.752 − 2 |
| 22 | 11 | −5.787 − 1 | 1.274 + 0 | 9.265 − 2 |
| 22 | 10 | −4.851 − 1 | 5.164 − 1 | 9.152 − 2 |
| 22 | 9 | 7.229 − 1 | −5.010 + 0 | 2.542 − 2 |
| 22 | 8 | 1.371 + 0 | −9.158 + 0 | 1.270 − 3 |
| 22 | 7 | 2.660 + 0 | −1.596 + 1 | −6.125 − 2 |
| 22 | 6 | 1.062 + 0 | −1.050 + 1 | 4.368 − 2 |
| 22 | 5 | 8.395 − 1 | −1.022 + 1 | 6.094 − 2 |
| 22 | 4 | −1.250 + 0 | −2.347 + 0 | 1.908 − 1 |
| 22 | 3 | −6.680 − 1 | −5.272 + 0 | 1.582 − 1 |
| 22 | 2 | −1.652 + 0 | −1.272 + 0 | 2.134 − 1 |
| 22 | 1 | −1.207 + 0 | −3.391 + 0 | 1.863 − 1 |
| 22 | 0 | −2.401 + 0 | 1.277 + 0 | 2.578 − 1 |
| 23 | 23 | −9.824 − 3 | 2.758 + 0 | 4.235 − 1 |
| 23 | 22 | −9.558 + 0 | 1.929 + 1 | 9.715 − 1 |
| 23 | 21 | −1.436 + 1 | 4.560 + 1 | 1.112 + 0 |
| 23 | 20 | −1.292 + 1 | 4.346 + 1 | 9.555 − 1 |
| 23 | 19 | −9.646 + 0 | 3.202 + 1 | 7.223 − 1 |
| 23 | 18 | −6.789 + 0 | 2.201 + 1 | 5.243 − 1 |
| 23 | 17 | −4.228 + 0 | 1.270 + 1 | 3.533 − 1 |
| 23 | 16 | −2.973 + 0 | 8.720 + 0 | 2.617 − 1 |
| 23 | 15 | −2.409 + 0 | 6.931 + 0 | 2.211 − 1 |
| 23 | 14 | −7.813 − 1 | 8.482 − 1 | 1.175 − 1 |
| 23 | 13 | −1.076 + 0 | 2.474 + 0 | 1.298 − 1 |
| 23 | 12 | −6.443 − 1 | 9.810 − 1 | 1.012 − 1 |
| 23 | 11 | −1.005 + 0 | 2.708 + 0 | 1.191 − 1 |
| 23 | 10 | −9.677 − 2 | −1.326 + 0 | 6.836 − 2 |
| 23 | 9 | 3.263 − 1 | −3.781 + 0 | 5.050 − 2 |
| 23 | 8 | 1.434 + 0 | −9.628 + 0 | −3.157 − 3 |
| 23 | 7 | 1.096 + 0 | −9.616 + 0 | 2.996 − 2 |
| 23 | 6 | 1.243 + 0 | −1.151 + 1 | 3.339 − 2 |
| 23 | 5 | 3.603 − 2 | −7.125 + 0 | 1.078 − 1 |
| 23 | 4 | −3.361 − 1 | −6.121 + 0 | 1.322 − 1 |
| 23 | 3 | −1.047 + 0 | −3.879 + 0 | 1.790 − 1 |
| 23 | 2 | −2.527 + 0 | 1.841 + 0 | 2.677 − 1 |
| 23 | 1 | −2.473 + 0 | 1.239 + 0 | 2.644 − 1 |
| 23 | 0 | −3.711 + 0 | 6.484 + 0 | 3.337 − 1 |

**Table A1** (*Continued.*)

| $\nu_i$ | $\nu_f$ | $a1$ | $a2$ | $a3$ |
|---|---|---|---|---|
| 24 | 24 | −1.686 + 0 | 9.535 + 0 | 5.241 − 1 |
| 24 | 23 | −8.838 + 0 | 1.650 + 1 | 9.263 − 1 |
| 24 | 22 | −1.384 + 1 | 4.341 + 1 | 1.082 + 0 |
| 24 | 21 | −1.285 + 1 | 4.293 + 1 | 9.527 − 1 |
| 24 | 20 | −9.737 + 0 | 3.240 + 1 | 7.248 − 1 |
| 24 | 19 | −5.843 + 0 | 1.804 + 1 | 4.652 − 1 |
| 24 | 18 | −4.838 + 0 | 1.481 + 1 | 3.909 − 1 |
| 24 | 17 | −3.247 + 0 | 9.352 + 0 | 2.807 − 1 |
| 24 | 16 | −1.965 + 0 | 4.887 + 0 | 1.937 − 1 |
| 24 | 15 | −2.598 + 0 | 7.885 + 0 | 2.261 − 1 |
| 24 | 14 | −8.104 − 1 | 7.822 − 1 | 1.174 − 1 |
| 24 | 13 | −3.463 − 1 | −7.984 − 1 | 8.616 − 2 |
| 24 | 12 | −1.624 − 1 | −1.481 + 0 | 7.513 − 2 |
| 24 | 11 | 1.995 − 2 | −1.738 + 0 | 5.818 − 2 |
| 24 | 10 | 1.787 − 1 | −2.640 + 0 | 5.058 − 2 |
| 24 | 9 | 4.413 − 1 | −4.404 + 0 | 4.205 − 2 |
| 24 | 8 | 1.350 + 0 | −9.247 + 0 | −2.597 − 3 |
| 24 | 7 | 1.310 + 0 | −1.066 + 1 | 1.596 − 2 |
| 24 | 6 | 1.118 + 0 | −1.103 + 1 | 3.679 − 2 |
| 24 | 5 | 9.631 − 2 | −7.551 + 0 | 1.023 − 1 |
| 24 | 4 | −6.671 − 1 | −4.864 + 0 | 1.495 − 1 |
| 24 | 3 | −1.349 + 0 | −2.408 + 0 | 1.896 − 1 |
| 24 | 2 | −2.168 + 0 | 2.095 − 2 | 2.464 − 1 |
| 24 | 1 | −2.507 + 0 | 1.230 + 0 | 2.637 − 1 |
| 24 | 0 | −4.264 + 0 | 8.588 + 0 | 3.643 − 1 |
| 25 | 25 | −2.408 + 0 | 1.197 + 1 | 5.757 − 1 |
| 25 | 24 | −8.519 + 0 | 1.552 + 1 | 9.036 − 1 |
| 25 | 23 | −1.423 + 1 | 4.529 + 1 | 1.100 + 0 |
| 25 | 22 | −1.201 + 1 | 3.988 + 1 | 8.962 − 1 |
| 25 | 21 | −9.447 + 0 | 3.126 + 1 | 7.053 − 1 |
| 25 | 20 | −5.849 + 0 | 1.800 + 1 | 4.643 − 1 |
| 25 | 19 | −5.115 + 0 | 1.601 + 1 | 4.039 − 1 |
| 25 | 18 | −3.543 + 0 | 1.025 + 1 | 2.989 − 1 |
| 25 | 17 | −3.212 + 0 | 9.698 + 0 | 2.686 − 1 |
| 25 | 16 | −1.805 + 0 | 4.208 + 0 | 1.800 − 1 |
| 25 | 15 | −9.966 − 1 | 1.174 + 0 | 1.283 − 1 |
| 25 | 14 | −8.841 − 1 | 1.044 + 0 | 1.175 − 1 |
| 25 | 13 | 4.113 − 1 | −4.253 + 0 | 4.046 − 2 |
| 25 | 12 | −7.312 − 1 | 8.405 − 1 | 1.058 − 1 |
| 25 | 11 | 6.765 − 2 | −2.305 + 0 | 5.576 − 2 |
| 25 | 10 | 1.911 − 1 | −2.939 + 0 | 4.931 − 2 |
| 25 | 9 | 6.425 − 1 | −5.377 + 0 | 2.772 − 2 |
| 25 | 8 | 1.272 + 0 | −9.016 + 0 | 1.107 − 5 |
| 25 | 7 | 1.925 + 0 | −1.345 + 1 | −2.248 − 2 |
| 25 | 6 | −2.282 − 1 | −5.480 + 0 | 1.130 − 1 |
| 25 | 5 | −6.457 − 1 | −4.666 + 0 | 1.450 − 1 |
| 25 | 4 | −1.152 + 0 | −2.976 + 0 | 1.750 − 1 |
| 25 | 3 | −2.050 + 0 | 1.238 − 1 | 2.314 − 1 |
| 25 | 2 | −2.563 + 0 | 1.350 + 0 | 2.694 − 1 |
| 25 | 1 | −3.123 + 0 | 3.331 + 0 | 3.015 − 1 |
| 25 | 0 | −4.193 + 0 | 7.749 + 0 | 3.627 − 1 |
| 26 | 26 | −1.387 + 1 | 4.935 + 1 | 1.444 + 0 |
| 26 | 25 | −7.943 + 0 | 1.354 + 1 | 8.644 − 1 |
| 26 | 24 | −1.320 + 1 | 4.158 + 1 | 1.031 + 0 |
| 26 | 23 | −1.143 + 1 | 3.753 + 1 | 8.595 − 1 |
| 26 | 22 | −8.823 + 0 | 2.869 + 1 | 6.671 − 1 |
| 26 | 21 | −7.249 + 0 | 2.367 + 1 | 5.465 − 1 |
| 26 | 20 | −5.094 + 0 | 1.608 + 1 | 3.975 − 1 |
| 26 | 19 | −4.322 + 0 | 1.341 + 1 | 3.423 − 1 |
| 26 | 18 | −3.213 + 0 | 9.331 + 0 | 2.686 − 1 |
| 26 | 17 | −2.373 + 0 | 5.916 + 0 | 2.181 − 1 |
| 26 | 16 | −1.904 + 0 | 4.472 + 0 | 1.832 − 1 |
| 26 | 15 | −9.573 − 1 | 6.005 − 1 | 1.278 − 1 |
| 26 | 14 | −1.093 + 0 | 1.328 + 0 | 1.338 − 1 |
| 26 | 13 | 7.274 − 1 | −5.768 + 0 | 2.070 − 2 |
| 26 | 12 | 3.128 − 1 | −3.548 + 0 | 3.951 − 2 |
| 26 | 11 | 4.096 − 1 | −3.856 + 0 | 3.423 − 2 |
| 26 | 10 | −3.330 − 1 | −6.379 − 1 | 7.490 − 2 |
| 26 | 9 | −1.275 − 1 | −2.157 + 0 | 6.912 − 2 |
| 26 | 8 | 1.077 + 0 | −8.569 + 0 | 1.311 − 2 |
| 26 | 7 | 6.734 − 1 | −8.211 + 0 | 4.732 − 2 |
| 26 | 6 | 1.165 + 0 | −1.144 + 1 | 2.847 − 2 |
| 26 | 5 | −7.448 − 1 | −4.167 + 0 | 1.452 − 1 |
| 26 | 4 | −2.167 + 0 | 8.234 − 1 | 2.361 − 1 |
| 26 | 3 | −2.433 + 0 | 1.212 + 0 | 2.560 − 1 |

**Table A1** (*Continued.*)

| $\nu_i$ | $\nu_f$ | $a1$ | $a2$ | $a3$ |
|---|---|---|---|---|
| 26 | 2 | −3.349 + 0 | 4.369 + 0 | 3.129 − 1 |
| 26 | 1 | −3.496 + 0 | 4.433 + 0 | 3.254 − 1 |
| 26 | 0 | −4.662 + 0 | 9.550 + 0 | 3.858 − 1 |
| 27 | 27 | −2.936 + 0 | 1.454 + 1 | 5.965 − 1 |
| 27 | 26 | −8.065 + 0 | 1.417 + 1 | 8.707 − 1 |
| 27 | 25 | −1.300 + 1 | 4.066 + 1 | 1.022 + 0 |
| 27 | 24 | −1.162 + 1 | 3.878 + 1 | 8.654 − 1 |
| 27 | 23 | −8.677 + 0 | 2.842 + 1 | 6.524 − 1 |
| 27 | 22 | −7.247 + 0 | 2.399 + 1 | 5.413 − 1 |
| 27 | 21 | −5.611 + 0 | 1.816 + 1 | 4.271 − 1 |
| 27 | 20 | −5.266 + 0 | 1.711 + 1 | 3.989 − 1 |
| 27 | 19 | −4.212 + 0 | 1.310 + 1 | 3.300 − 1 |
| 27 | 18 | −3.403 + 0 | 9.863 + 0 | 2.801 − 1 |
| 27 | 17 | −1.619 + 0 | 2.685 + 0 | 1.705 − 1 |
| 27 | 16 | −1.189 + 0 | 1.203 + 0 | 1.411 − 1 |
| 27 | 15 | −7.376 − 1 | −4.136 − 1 | 1.110 − 1 |
| 27 | 14 | −4.477 − 1 | −1.544 + 0 | 9.486 − 2 |
| 27 | 13 | −3.906 − 1 | −1.587 + 0 | 8.919 − 2 |
| 27 | 12 | 1.733 − 1 | −3.522 + 0 | 5.170 − 2 |
| 27 | 11 | 4.686 − 1 | −4.214 + 0 | 2.833 − 2 |
| 27 | 10 | −5.457 − 1 | −1.615 − 1 | 8.850 − 2 |
| 27 | 9 | −4.018 − 1 | −1.342 + 0 | 8.594 − 2 |
| 27 | 8 | 8.418 − 1 | −7.948 + 0 | 2.719 − 2 |
| 27 | 7 | 9.086 − 1 | −9.309 + 0 | 3.210 − 2 |
| 27 | 6 | 2.521 − 1 | −7.851 + 0 | 8.168 − 2 |
| 27 | 5 | −5.008 − 1 | −5.593 + 0 | 1.318 − 1 |
| 27 | 4 | −2.256 + 0 | 1.288 + 0 | 2.359 − 1 |
| 27 | 3 | −2.728 + 0 | 2.280 + 0 | 2.716 − 1 |
| 27 | 2 | −2.842 + 0 | 2.021 + 0 | 2.830 − 1 |
| 27 | 1 | −3.245 + 0 | 3.143 + 0 | 3.087 − 1 |
| 27 | 0 | −5.298 + 0 | 1.147 + 1 | 4.287 − 1 |
| 28 | 28 | −6.854 + 0 | 2.829 + 1 | 8.716 − 1 |
| 28 | 27 | −6.769 + 0 | 9.560 + 0 | 7.839 − 1 |
| 28 | 26 | −1.156 + 1 | 3.520 + 1 | 9.291 − 1 |
| 28 | 25 | −1.054 + 1 | 3.436 + 1 | 7.998 − 1 |
| 28 | 24 | −8.012 + 0 | 2.584 + 1 | 6.104 − 1 |
| 28 | 23 | −7.328 + 0 | 2.456 + 1 | 5.416 − 1 |
| 28 | 22 | −6.270 + 0 | 2.076 + 1 | 4.654 − 1 |
| 28 | 21 | −4.407 + 0 | 1.355 + 1 | 3.458 − 1 |
| 28 | 20 | −3.926 + 0 | 1.212 + 1 | 3.067 − 1 |
| 28 | 19 | −3.653 + 0 | 1.071 + 1 | 2.929 − 1 |
| 28 | 18 | −2.078 + 0 | 4.225 + 0 | 1.975 − 1 |
| 28 | 17 | −1.776 + 0 | 3.020 + 0 | 1.791 − 1 |
| 28 | 16 | −1.699 + 0 | 2.995 + 0 | 1.714 − 1 |
| 28 | 15 | −3.826 − 1 | −2.205 + 0 | 9.077 − 2 |
| 28 | 14 | −1.006 + 0 | 7.585 − 1 | 1.235 − 1 |
| 28 | 13 | −5.147 − 1 | −1.081 + 0 | 9.270 − 2 |
| 28 | 12 | 2.755 − 1 | −4.132 + 0 | 4.354 − 2 |
| 28 | 11 | 1.188 − 1 | −3.122 + 0 | 4.886 − 2 |
| 28 | 10 | −6.571 − 1 | 2.862 − 1 | 9.196 − 2 |
| 28 | 9 | −5.736 − 1 | −8.745 − 1 | 9.620 − 2 |
| 28 | 8 | 6.911 − 3 | −4.604 + 0 | 7.328 − 2 |
| 28 | 7 | −1.137 − 1 | −5.410 + 0 | 9.256 − 2 |
| 28 | 6 | 4.267 − 1 | −8.670 + 0 | 6.814 − 2 |
| 28 | 5 | −1.762 + 0 | −4.727 − 1 | 2.042 − 1 |
| 28 | 4 | −2.246 + 0 | 8.279 − 1 | 2.364 − 1 |
| 28 | 3 | −3.285 + 0 | 4.408 + 0 | 3.025 − 1 |
| 28 | 2 | −2.204 + 0 | −8.758 − 1 | 2.436 − 1 |
| 28 | 1 | −3.309 + 0 | 3.017 + 0 | 3.124 − 1 |
| 28 | 0 | −6.309 + 0 | 1.537 + 1 | 4.874 − 1 |
| 29 | 29 | −2.011 + 0 | 1.093 + 1 | 5.366 − 1 |
| 29 | 28 | −7.506 + 0 | 1.293 + 1 | 8.249 − 1 |
| 29 | 27 | −1.170 + 1 | 3.637 + 1 | 9.299 − 1 |
| 29 | 26 | −1.069 + 1 | 3.547 + 1 | 8.032 − 1 |
| 29 | 25 | −8.502 + 0 | 2.833 + 1 | 6.325 − 1 |
| 29 | 24 | −6.701 + 0 | 2.204 + 1 | 5.028 − 1 |
| 29 | 23 | −5.675 + 0 | 1.854 + 1 | 4.255 − 1 |
| 29 | 22 | −4.477 + 0 | 1.390 + 1 | 3.465 − 1 |
| 29 | 21 | −3.584 + 0 | 1.006 + 1 | 2.928 − 1 |
| 29 | 20 | −2.956 + 0 | 7.775 + 0 | 2.494 − 1 |
| 29 | 19 | −3.020 + 0 | 7.811 + 0 | 2.545 − 1 |
| 29 | 18 | −1.665 + 0 | 2.086 + 0 | 1.757 − 1 |
| 29 | 17 | −1.345 + 0 | 8.559 − 1 | 1.542 − 1 |
| 29 | 16 | −2.681 − 1 | −2.999 + 0 | 8.323 − 2 |
| 29 | 15 | −1.094 + 0 | 2.698 − 1 | 1.353 − 1 |

**Table A1** (*Continued.*)

| $\nu_i$ | $\nu_f$ | $a1$ | $a2$ | $a3$ |
|---|---|---|---|---|
| 29 | 14 | 3.402 − 2 | −3.816 + 0 | 6.146 − 2 |
| 29 | 13 | −3.557 − 1 | −2.087 + 0 | 8.348 − 2 |
| 29 | 12 | 1.871 − 1 | −4.065 + 0 | 4.908 − 2 |
| 29 | 11 | −7.952 − 1 | 6.538 − 1 | 9.939 − 2 |
| 29 | 10 | −1.548 + 0 | 3.513 + 0 | 1.469 − 1 |
| 29 | 9 | −2.427 − 1 | −2.714 + 0 | 7.804 − 2 |
| 29 | 8 | −1.239 + 0 | 1.735 − 1 | 1.492 − 1 |
| 29 | 7 | −2.651 − 1 | −4.751 + 0 | 9.729 − 2 |
| 29 | 6 | −2.053 + 0 | 1.368 + 0 | 2.154 − 1 |
| 29 | 5 | −2.334 + 0 | 1.414 + 0 | 2.406 − 1 |
| 29 | 4 | −3.616 + 0 | 6.527 + 0 | 3.127 − 1 |
| 29 | 3 | −3.576 + 0 | 5.201 + 0 | 3.202 − 1 |
| 29 | 2 | −4.007 + 0 | 6.337 + 0 | 3.491 − 1 |
| 29 | 1 | −4.153 + 0 | 6.453 + 0 | 3.592 − 1 |
| 29 | 0 | −5.800 + 0 | 1.279 + 1 | 4.593 − 1 |
| 30 | 30 | −8.252 + 0 | 3.474 + 1 | 9.408 − 1 |
| 30 | 29 | −5.970 + 0 | 7.397 + 0 | 7.231 − 1 |
| 30 | 28 | −1.066 + 1 | 3.256 + 1 | 8.630 − 1 |
| 30 | 27 | −9.559 + 0 | 3.136 + 1 | 7.261 − 1 |
| 30 | 26 | −7.770 + 0 | 2.568 + 1 | 5.847 − 1 |
| 30 | 25 | −6.142 + 0 | 2.013 + 1 | 4.629 − 1 |
| 30 | 24 | −4.384 + 0 | 1.357 + 1 | 3.427 − 1 |
| 30 | 23 | −4.016 + 0 | 1.222 + 1 | 3.144 − 1 |
| 30 | 22 | −3.263 + 0 | 8.564 + 0 | 2.732 − 1 |
| 30 | 21 | −3.704 + 0 | 1.044 + 1 | 2.952 − 1 |
| 30 | 20 | −2.179 + 0 | 4.205 + 0 | 2.025 − 1 |
| 30 | 19 | −2.127 + 0 | 3.897 + 0 | 1.991 − 1 |
| 30 | 18 | −1.260 + 0 | 8.309 − 2 | 1.506 − 1 |
| 30 | 17 | −6.577 − 1 | −2.117 + 0 | 1.101 − 1 |
| 30 | 16 | −9.451 − 1 | −4.696 − 1 | 1.234 − 1 |
| 30 | 15 | −1.408 + 0 | 1.744 + 0 | 1.473 − 1 |
| 30 | 14 | −9.770 − 1 | 3.179 − 1 | 1.178 − 1 |
| 30 | 13 | −1.073 + 0 | 8.741 − 1 | 1.224 − 1 |
| 30 | 12 | −3.866 − 1 | −1.628 + 0 | 7.773 − 2 |
| 30 | 11 | −6.139 − 1 | −7.260 − 1 | 9.147 − 2 |
| 30 | 10 | −2.735 + 0 | 7.894 + 0 | 2.194 − 1 |
| 30 | 9 | −1.622 + 0 | 2.769 + 0 | 1.584 − 1 |
| 30 | 8 | −1.697 + 0 | 2.071 + 0 | 1.713 − 1 |
| 30 | 7 | −1.680 + 0 | 9.295 − 1 | 1.776 − 1 |
| 30 | 6 | −1.961 + 0 | 9.184 − 1 | 2.049 − 1 |
| 30 | 5 | −2.164 + 0 | 8.591 − 1 | 2.226 − 1 |
| 30 | 4 | −4.671 + 0 | 1.066 + 1 | 3.726 − 1 |
| 30 | 3 | −3.480 + 0 | 4.660 + 0 | 3.104 − 1 |
| 30 | 2 | −3.748 + 0 | 4.771 + 0 | 3.343 − 1 |
| 30 | 1 | −3.916 + 0 | 4.961 + 0 | 3.470 − 1 |
| 30 | 0 | −6.699 + 0 | 1.638 + 1 | 5.091 − 1 |
| 31 | 31 | −1.818 + 0 | 9.880 + 0 | 5.223 − 1 |
| 31 | 30 | −5.726 + 0 | 6.726 + 0 | 7.050 − 1 |
| 31 | 29 | −1.065 + 1 | 3.338 + 1 | 8.517 − 1 |
| 31 | 28 | −7.935 + 0 | 2.503 + 1 | 6.255 − 1 |
| 31 | 27 | −7.687 + 0 | 2.595 + 1 | 5.703 − 1 |
| 31 | 26 | −5.911 + 0 | 1.943 + 1 | 4.451 − 1 |
| 31 | 25 | −3.788 + 0 | 1.114 + 1 | 3.052 − 1 |
| 31 | 24 | −4.866 + 0 | 1.599 + 1 | 3.597 − 1 |
| 31 | 23 | −3.013 + 0 | 8.206 + 0 | 2.463 − 1 |
| 31 | 22 | −3.805 + 0 | 1.088 + 1 | 2.999 − 1 |
| 31 | 21 | −1.689 + 0 | 1.714 + 0 | 1.767 − 1 |
| 31 | 20 | −1.166 + 0 | −2.644 − 1 | 1.413 − 1 |
| 31 | 19 | −7.677 − 1 | −2.010 + 0 | 1.179 − 1 |
| 31 | 18 | −1.439 + 0 | 7.504 − 1 | 1.575 − 1 |
| 31 | 17 | −6.905 − 1 | −2.139 + 0 | 1.104 − 1 |
| 31 | 16 | −1.649 + 0 | 1.912 + 0 | 1.675 − 1 |
| 31 | 15 | −2.002 + 0 | 3.823 + 0 | 1.832 − 1 |
| 31 | 14 | −1.594 + 0 | 2.486 + 0 | 1.549 − 1 |
| 31 | 13 | −1.843 + 0 | 3.759 + 0 | 1.672 − 1 |
| 31 | 12 | −1.421 + 0 | 2.127 + 0 | 1.416 − 1 |
| 31 | 11 | −1.303 + 0 | 1.471 + 0 | 1.379 − 1 |
| 31 | 10 | −4.010 + 0 | 1.260 + 1 | 2.989 − 1 |
| 31 | 9 | −1.299 + 0 | 1.183 + 0 | 1.369 − 1 |
| 31 | 8 | −2.019 + 0 | 3.371 + 0 | 1.860 − 1 |
| 31 | 7 | −3.442 + 0 | 7.725 + 0 | 2.849 − 1 |
| 31 | 6 | −2.641 + 0 | 3.338 + 0 | 2.459 − 1 |
| 31 | 5 | −5.435 + 0 | 1.398 + 1 | 4.182 − 1 |
| 31 | 4 | −4.172 + 0 | 8.140 + 0 | 3.447 − 1 |
| 31 | 3 | −2.995 + 0 | 2.182 + 0 | 2.842 − 1 |

**Table A1** (*Continued.*)

| $\nu_i$ | $\nu_f$ | $a1$ | $a2$ | $a3$ |
|---|---|---|---|---|
| 31 | 2 | −3.894 + 0 | 5.104 + 0 | 3.418 − 1 |
| 31 | 1 | −4.146 + 0 | 6.122 + 0 | 3.537 − 1 |
| 31 | 0 | −4.678 + 0 | 7.188 + 0 | 3.943 − 1 |
| 32 | 32 | −6.021 + 0 | 2.304 + 1 | 8.502 − 1 |
| 32 | 31 | −5.535 + 0 | 6.908 + 0 | 6.820 − 1 |
| 32 | 30 | −1.025 + 1 | 3.201 + 1 | 8.255 − 1 |
| 32 | 29 | −8.645 + 0 | 2.872 + 1 | 6.586 − 1 |
| 32 | 28 | −6.132 + 0 | 2.025 + 1 | 4.685 − 1 |
| 32 | 27 | −6.503 + 0 | 2.230 + 1 | 4.732 − 1 |
| 32 | 26 | −4.108 + 0 | 1.270 + 1 | 3.185 − 1 |
| 32 | 25 | −3.226 + 0 | 9.063 + 0 | 2.618 − 1 |
| 32 | 24 | −3.435 + 0 | 9.835 + 0 | 2.702 − 1 |
| 32 | 23 | −2.603 + 0 | 6.280 + 0 | 2.178 − 1 |
| 32 | 22 | −1.747 + 0 | 2.329 + 0 | 1.724 − 1 |
| 32 | 21 | −1.565 + 0 | 1.083 + 0 | 1.656 − 1 |
| 32 | 20 | −7.203 − 1 | −2.380 + 0 | 1.129 − 1 |
| 32 | 19 | −2.080 + 0 | 3.103 + 0 | 1.949 − 1 |
| 32 | 18 | −1.696 + 0 | 1.818 + 0 | 1.674 − 1 |
| 32 | 17 | −1.842 + 0 | 2.280 + 0 | 1.778 − 1 |
| 32 | 16 | −1.697 + 0 | 2.091 + 0 | 1.641 − 1 |
| 32 | 15 | −1.412 + 0 | 1.305 + 0 | 1.441 − 1 |
| 32 | 14 | −1.630 + 0 | 2.511 + 0 | 1.544 − 1 |
| 32 | 13 | −2.151 + 0 | 4.846 + 0 | 1.842 − 1 |
| 32 | 12 | −2.383 + 0 | 6.153 + 0 | 1.916 − 1 |
| 32 | 11 | −1.573 + 0 | 2.513 + 0 | 1.483 − 1 |
| 32 | 10 | −1.781 + 0 | 3.133 + 0 | 1.630 − 1 |
| 32 | 9 | −1.578 + 0 | 2.010 + 0 | 1.520 − 1 |
| 32 | 8 | −2.726 + 0 | 5.401 + 0 | 2.341 − 1 |
| 32 | 7 | −3.633 + 0 | 8.284 + 0 | 2.942 − 1 |
| 32 | 6 | −4.218 + 0 | 9.856 + 0 | 3.325 − 1 |
| 32 | 5 | −5.117 + 0 | 1.301 + 1 | 3.885 − 1 |
| 32 | 4 | −4.937 + 0 | 1.120 + 1 | 3.867 − 1 |
| 32 | 3 | −6.064 + 0 | 1.480 + 1 | 4.610 − 1 |
| 32 | 2 | −4.180 + 0 | 6.748 + 0 | 3.478 − 1 |
| 32 | 1 | −5.268 + 0 | 1.100 + 1 | 4.104 − 1 |
| 32 | 0 | −5.784 + 0 | 1.225 + 1 | 4.484 − 1 |
| 33 | 33 | −6.409 + 0 | 2.776 + 1 | 8.116 − 1 |
| 33 | 32 | −5.376 + 0 | 6.963 + 0 | 6.654 − 1 |
| 33 | 31 | −1.068 + 1 | 3.481 + 1 | 8.367 − 1 |
| 33 | 30 | −7.146 + 0 | 2.338 + 1 | 5.576 − 1 |
| 33 | 29 | −5.028 + 0 | 1.611 + 1 | 3.961 − 1 |
| 33 | 28 | −5.455 + 0 | 1.830 + 1 | 4.081 − 1 |
| 33 | 27 | −3.524 + 0 | 1.086 + 1 | 2.747 − 1 |
| 33 | 26 | −2.848 + 0 | 7.534 + 0 | 2.378 − 1 |
| 33 | 25 | −1.079 + 0 | −8.215 − 2 | 1.300 − 1 |
| 33 | 24 | −1.047 + 0 | −5.416 − 1 | 1.294 − 1 |
| 33 | 23 | −1.599 + 0 | 1.526 + 0 | 1.605 − 1 |
| 33 | 22 | −2.431 + 0 | 4.665 + 0 | 2.134 − 1 |
| 33 | 21 | −2.525 + 0 | 4.812 + 0 | 2.208 − 1 |
| 33 | 20 | −1.469 + 0 | 2.417 − 1 | 1.592 − 1 |
| 33 | 19 | −1.722 + 0 | 1.253 + 0 | 1.743 − 1 |
| 33 | 18 | −2.105 + 0 | 3.004 + 0 | 1.946 − 1 |
| 33 | 17 | −2.495 + 0 | 4.772 + 0 | 2.155 − 1 |
| 33 | 16 | −1.201 + 0 | −3.746 − 1 | 1.364 − 1 |
| 33 | 15 | −3.028 + 0 | 7.592 + 0 | 2.413 − 1 |
| 33 | 14 | −2.861 + 0 | 6.865 + 0 | 2.321 − 1 |
| 33 | 13 | −4.563 − 1 | −2.530 + 0 | 8.250 − 2 |
| 33 | 12 | −7.781 − 1 | −8.028 − 1 | 9.500 − 2 |
| 33 | 11 | −3.043 + 0 | 8.282 + 0 | 2.354 − 1 |
| 33 | 10 | −2.348 + 0 | 5.194 + 0 | 1.942 − 1 |
| 33 | 9 | −4.662 + 0 | 1.418 + 1 | 3.369 − 1 |
| 33 | 8 | −4.473 + 0 | 1.225 + 1 | 3.368 − 1 |
| 33 | 7 | −3.528 + 0 | 7.700 + 0 | 2.839 − 1 |
| 33 | 6 | −6.848 + 0 | 2.004 + 1 | 4.952 − 1 |
| 33 | 5 | −4.759 + 0 | 1.086 + 1 | 3.708 − 1 |
| 33 | 4 | −5.582 + 0 | 1.338 + 1 | 4.244 − 1 |
| 33 | 2 | −4.596 + 0 | 8.040 + 0 | 3.731 − 1 |
| 33 | 1 | −4.734 + 0 | 8.622 + 0 | 3.752 − 1 |
| 33 | 0 | −5.382 + 0 | 1.057 + 1 | 4.202 − 1 |
| 34 | 34 | −4.532 + 0 | 2.074 + 1 | 6.842 − 1 |
| 34 | 33 | −5.617 + 0 | 9.091 + 0 | 6.662 − 1 |
| 34 | 32 | −1.031 + 1 | 3.416 + 1 | 8.056 − 1 |
| 34 | 31 | −8.016 + 0 | 2.763 + 1 | 5.997 − 1 |
| 34 | 30 | −7.373 + 0 | 2.629 + 1 | 5.300 − 1 |
| 34 | 29 | −4.392 + 0 | 1.473 + 1 | 3.311 − 1 |

**Table A1** (*Continued.*)

| $\nu_i$ | $\nu_f$ | $a1$ | $a2$ | $a3$ |
|---|---|---|---|---|
| 34 | 28 | −2.623 + 0 | 7.209 + 0 | 2.220 − 1 |
| 34 | 27 | −2.315 + 0 | 5.756 + 0 | 1.970 − 1 |
| 34 | 26 | −2.310 + 0 | 4.772 + 0 | 2.065 − 1 |
| 34 | 25 | −4.591 − 1 | −3.191 + 0 | 9.469 − 2 |
| 34 | 24 | −1.363 + 0 | 5.042 − 1 | 1.453 − 1 |
| 34 | 23 | −1.341 + 0 | −1.376 − 1 | 1.476 − 1 |
| 34 | 22 | −1.508 + 0 | 7.172 − 1 | 1.542 − 1 |
| 34 | 21 | −2.735 + 0 | 5.380 + 0 | 2.308 − 1 |
| 34 | 20 | −1.660 + 0 | 8.587 − 1 | 1.663 − 1 |
| 34 | 19 | −1.916 + 0 | 2.064 + 0 | 1.790 − 1 |
| 34 | 18 | −1.770 + 0 | 1.267 + 0 | 1.728 − 1 |
| 34 | 17 | −1.638 + 0 | 8.953 − 1 | 1.645 − 1 |
| 34 | 16 | −3.728 + 0 | 9.723 + 0 | 2.875 − 1 |
| 34 | 15 | −2.328 + 0 | 4.454 + 0 | 1.968 − 1 |
| 34 | 14 | −2.891 + 0 | 7.127 + 0 | 2.264 − 1 |
| 34 | 13 | −2.273 + 0 | 4.673 + 0 | 1.895 − 1 |
| 34 | 12 | −2.391 + 0 | 5.321 + 0 | 1.938 − 1 |
| 34 | 11 | −4.920 + 0 | 1.551 + 1 | 3.469 − 1 |
| 34 | 10 | −2.536 + 0 | 5.524 + 0 | 2.065 − 1 |
| 34 | 9 | −2.807 + 0 | 5.824 + 0 | 2.311 − 1 |
| 34 | 8 | −4.390 + 0 | 1.145 + 1 | 3.328 − 1 |
| 34 | 7 | −5.251 + 0 | 1.415 + 1 | 3.902 − 1 |
| 34 | 6 | −3.495 + 0 | 6.187 + 0 | 2.883 − 1 |
| 34 | 5 | −6.947 + 0 | 1.922 + 1 | 5.046 − 1 |
| 34 | 4 | −7.177 + 0 | 1.958 + 1 | 5.195 − 1 |
| 34 | 3 | −5.691 + 0 | 1.248 + 1 | 4.376 − 1 |
| 34 | 2 | −5.309 + 0 | 1.066 + 1 | 4.143 − 1 |
| 34 | 1 | −3.328 + 0 | 2.308 + 0 | 2.953 − 1 |
| 34 | 0 | −5.875 + 0 | 1.200 + 1 | 4.525 − 1 |
| 35 | 35 | 1.409 + 1 | −6.296 + 1 | −2.376 − 1 |
| 35 | 34 | −5.402 + 0 | 9.525 + 0 | 6.352 − 1 |
| 35 | 33 | −1.037 + 1 | 3.554 + 1 | 7.940 − 1 |
| 35 | 32 | −7.896 + 0 | 2.801 + 1 | 5.822 − 1 |
| 35 | 31 | −6.193 + 0 | 2.188 + 1 | 4.520 − 1 |
| 35 | 30 | −3.316 + 0 | 1.046 + 1 | 2.648 − 1 |
| 35 | 29 | −2.713 + 0 | 8.285 + 0 | 2.135 − 1 |
| 35 | 28 | −2.091 + 0 | 4.650 + 0 | 1.848 − 1 |
| 35 | 27 | −7.684 − 1 | −1.066 + 0 | 1.025 − 1 |
| 35 | 26 | −4.030 − 1 | −3.122 + 0 | 8.357 − 2 |
| 35 | 25 | 4.573 − 1 | −7.170 + 0 | 3.325 − 2 |
| 35 | 24 | −4.917 − 1 | −3.521 + 0 | 8.956 − 2 |
| 35 | 23 | −7.939 − 1 | −2.578 + 0 | 1.097 − 1 |
| 35 | 22 | −2.593 + 0 | 4.344 + 0 | 2.216 − 1 |
| 35 | 21 | −2.471 + 0 | 3.806 + 0 | 2.131 − 1 |
| 35 | 20 | −7.778 − 1 | −3.277 + 0 | 1.129 − 1 |
| 35 | 19 | −1.485 + 0 | −2.635 − 1 | 1.534 − 1 |
| 35 | 18 | −1.601 + 0 | 3.671 − 1 | 1.567 − 1 |
| 35 | 17 | −2.112 + 0 | 2.770 + 0 | 1.845 − 1 |
| 35 | 16 | −2.182 + 0 | 3.264 + 0 | 1.877 − 1 |
| 35 | 15 | −4.594 + 0 | 1.354 + 1 | 3.280 − 1 |
| 35 | 14 | −3.477 + 0 | 9.374 + 0 | 2.561 − 1 |
| 35 | 13 | −5.766 + 0 | 1.911 + 1 | 3.904 − 1 |
| 35 | 12 | −3.133 + 0 | 7.794 + 0 | 2.393 − 1 |
| 35 | 11 | −2.993 + 0 | 6.948 + 0 | 2.339 − 1 |
| 35 | 10 | −2.343 + 0 | 4.501 + 0 | 1.908 − 1 |
| 35 | 9 | −6.051 + 0 | 1.898 + 1 | 4.191 − 1 |
| 35 | 8 | −4.078 + 0 | 9.639 + 0 | 3.135 − 1 |
| 35 | 7 | −5.043 + 0 | 1.303 + 1 | 3.722 − 1 |
| 35 | 6 | −5.700 + 0 | 1.509 + 1 | 4.156 − 1 |
| 35 | 5 | −5.753 + 0 | 1.427 + 1 | 4.252 − 1 |
| 35 | 4 | −5.183 + 0 | 1.121 + 1 | 3.942 − 1 |
| 35 | 3 | −5.636 + 0 | 1.192 + 1 | 4.315 − 1 |
| 35 | 2 | −7.374 + 0 | 1.905 + 1 | 5.311 − 1 |
| 35 | 1 | −5.257 + 0 | 1.008 + 1 | 4.046 − 1 |
| 35 | 0 | −5.623 + 0 | 1.072 + 1 | 4.346 − 1 |
| 36 | 36 | 1.363 + 1 | −5.891 + 1 | −2.581 − 1 |
| 36 | 35 | −6.789 + 0 | 1.645 + 1 | 7.052 − 1 |
| 36 | 34 | −1.067 + 1 | 3.783 + 1 | 7.964 − 1 |
| 36 | 33 | −8.936 + 0 | 3.298 + 1 | 6.349 − 1 |
| 36 | 32 | −5.199 + 0 | 1.863 + 1 | 3.816 − 1 |
| 36 | 31 | −4.051 + 0 | 1.442 + 1 | 2.937 − 1 |
| 36 | 30 | −2.424 + 0 | 6.917 + 0 | 1.991 − 1 |
| 36 | 29 | 5.124 − 1 | −5.147 + 0 | 1.112 − 2 |
| 36 | 28 | 6.667 − 2 | −4.427 + 0 | 4.838 − 2 |
| 36 | 27 | −7.384 − 1 | −2.009 + 0 | 1.036 − 1 |

**Table A1** (*Continued.*)

| $\nu_i$ | $\nu_f$ | $a1$ | $a2$ | $a3$ |
|---|---|---|---|---|
| 36 | 26 | −4.752 − 1 | −3.902 + 0 | 9.562 − 2 |
| 36 | 25 | 6.515 − 1 | −8.114 + 0 | 1.470 − 2 |
| 36 | 24 | −5.771 − 2 | −5.751 + 0 | 6.163 − 2 |
| 36 | 23 | 2.079 + 0 | −1.513 + 1 | −6.193 − 2 |
| 36 | 22 | −3.402 + 0 | 7.181 + 0 | 2.706 − 1 |
| 36 | 21 | −3.324 + 0 | 7.021 + 0 | 2.606 − 1 |
| 36 | 20 | −2.449 + 0 | 3.247 + 0 | 2.091 − 1 |
| 36 | 19 | −2.769 + 0 | 4.889 + 0 | 2.229 − 1 |
| 36 | 18 | −3.158 + 0 | 6.393 + 0 | 2.482 − 1 |
| 36 | 17 | −3.040 + 0 | 6.005 + 0 | 2.421 − 1 |
| 36 | 16 | −2.015 + 0 | 1.953 + 0 | 1.796 − 1 |
| 36 | 15 | −3.091 + 0 | 6.827 + 0 | 2.397 − 1 |
| 36 | 14 | −2.751 + 0 | 5.723 + 0 | 2.161 − 1 |
| 36 | 13 | −4.800 + 0 | 1.417 + 1 | 3.392 − 1 |
| 36 | 12 | −3.964 + 0 | 1.080 + 1 | 2.886 − 1 |
| 36 | 11 | −2.587 + 0 | 4.738 + 0 | 2.095 − 1 |
| 36 | 10 | −2.436 + 0 | 4.060 + 0 | 2.002 − 1 |
| 36 | 9 | −5.756 + 0 | 1.754 + 1 | 3.970 − 1 |
| 36 | 8 | −4.537 + 0 | 1.130 + 1 | 3.370 − 1 |
| 36 | 7 | −5.799 + 0 | 1.613 + 1 | 4.103 − 1 |
| 36 | 6 | −5.701 + 0 | 1.471 + 1 | 4.128 − 1 |
| 36 | 5 | −5.578 + 0 | 1.365 + 1 | 4.058 − 1 |
| 36 | 4 | −4.931 + 0 | 9.549 + 0 | 3.802 − 1 |
| 36 | 3 | −4.623 + 0 | 7.715 + 0 | 3.653 − 1 |
| 36 | 2 | −5.644 + 0 | 1.122 + 1 | 4.303 − 1 |
| 36 | 1 | −6.875 + 0 | 1.654 + 1 | 4.986 − 1 |
| 36 | 0 | −5.968 + 0 | 1.223 + 1 | 4.473 − 1 |
| 37 | 37 | 1.214 + 1 | −5.209 + 1 | −1.688 − 1 |
| 37 | 36 | −7.736 + 0 | 2.155 + 1 | 7.469 − 1 |
| 37 | 35 | −1.240 + 1 | 4.614 + 1 | 8.848 − 1 |
| 37 | 34 | −7.454 + 0 | 2.799 + 1 | 5.308 − 1 |
| 37 | 33 | −5.262 + 0 | 1.981 + 1 | 3.730 − 1 |
| 37 | 32 | −3.917 + 0 | 1.421 + 1 | 2.803 − 1 |
| 37 | 31 | −1.783 + 0 | 4.774 + 0 | 1.496 − 1 |
| 37 | 30 | 2.296 − 1 | −4.131 + 0 | 3.017 − 2 |
| 37 | 29 | 1.074 + 0 | −8.051 + 0 | −2.367 − 2 |
| 37 | 28 | 1.281 + 0 | −9.963 + 0 | −2.731 − 2 |
| 37 | 27 | 1.444 + 0 | −1.119 + 1 | −3.505 − 2 |
| 37 | 26 | 2.390 + 0 | −1.612 + 1 | −8.111 − 2 |
| 37 | 25 | −4.614 − 1 | −4.248 + 0 | 8.286 − 2 |
| 37 | 24 | −1.022 + 0 | −2.225 + 0 | 1.164 − 1 |
| 37 | 23 | −1.773 + 0 | 2.238 − 1 | 1.674 − 1 |
| 37 | 22 | −5.971 − 1 | −4.900 + 0 | 9.977 − 2 |
| 37 | 21 | −6.526 − 2 | −6.793 + 0 | 6.080 − 2 |
| 37 | 20 | −2.727 + 0 | 4.087 + 0 | 2.207 − 1 |
| 37 | 19 | −2.177 + 0 | 1.638 + 0 | 1.908 − 1 |
| 37 | 18 | −2.665 + 0 | 3.817 + 0 | 2.174 − 1 |
| 37 | 17 | −7.593 − 1 | −3.834 + 0 | 1.034 − 1 |
| 37 | 16 | −6.537 − 1 | −4.213 + 0 | 9.806 − 2 |
| 37 | 15 | −2.468 + 0 | 3.695 + 0 | 2.025 − 1 |
| 37 | 14 | −2.942 + 0 | 6.038 + 0 | 2.255 − 1 |
| 37 | 13 | −2.697 + 0 | 5.183 + 0 | 2.104 − 1 |
| 37 | 12 | −3.754 + 0 | 9.673 + 0 | 2.709 − 1 |
| 37 | 11 | −3.712 + 0 | 9.417 + 0 | 2.694 − 1 |
| 37 | 10 | −3.517 + 0 | 7.648 + 0 | 2.683 − 1 |
| 37 | 9 | −3.818 + 0 | 8.617 + 0 | 2.863 − 1 |
| 37 | 8 | −4.527 + 0 | 1.091 + 1 | 3.313 − 1 |
| 37 | 7 | −7.753 + 0 | 2.349 + 1 | 5.289 − 1 |
| 37 | 6 | −6.814 + 0 | 1.816 + 1 | 4.855 − 1 |
| 37 | 5 | −4.781 + 0 | 9.751 + 0 | 3.580 − 1 |
| 37 | 4 | −8.642 + 0 | 2.419 + 1 | 6.033 − 1 |
| 37 | 3 | −5.675 + 0 | 1.206 + 1 | 4.192 − 1 |
| 37 | 2 | −4.735 + 0 | 7.241 + 0 | 3.699 − 1 |
| 37 | 1 | −6.830 + 0 | 1.593 + 1 | 4.922 − 1 |
| 37 | 0 | −5.082 + 0 | 8.276 + 0 | 3.894 − 1 |
| 38 | 38 | 9.876 + 0 | −3.777 + 1 | −1.011 − 2 |
| 38 | 37 | −9.767 + 0 | 3.122 + 1 | 8.515 − 1 |
| 38 | 36 | −1.184 + 1 | 4.489 + 1 | 8.375 − 1 |
| 38 | 35 | −9.338 + 0 | 3.671 + 1 | 6.305 − 1 |
| 38 | 34 | −5.196 + 0 | 2.012 + 1 | 3.570 − 1 |
| 38 | 33 | −1.455 + 0 | 4.775 + 0 | 1.208 − 1 |
| 38 | 32 | −1.479 − 2 | −1.941 + 0 | 3.525 − 2 |
| 38 | 31 | 2.141 + 0 | −1.160 + 1 | −9.455 − 2 |
| 38 | 30 | 7.570 − 1 | −7.002 + 0 | −2.785 − 3 |
| 38 | 29 | 3.377 + 0 | −1.813 + 1 | −1.656 − 1 |

**Table A1** (*Continued.*)

| $\nu_i$ | $\nu_f$ | $a1$ | $a2$ | $a3$ |
|---|---|---|---|---|
| 38 | 28 | 4.520 + 0 | −2.397 + 1 | −2.218 − 1 |
| 38 | 27 | 3.205 + 0 | −1.880 + 1 | −1.477 − 1 |
| 38 | 26 | 1.634 + 0 | −1.318 + 1 | −4.672 − 2 |
| 38 | 25 | 1.049 + 0 | −1.099 + 1 | −1.127 − 2 |
| 38 | 24 | 1.008 + 0 | −1.137 + 1 | −4.203 − 3 |
| 38 | 23 | −1.279 + 0 | −2.244 + 0 | 1.334 − 1 |
| 38 | 22 | 5.309 − 1 | −9.825 + 0 | 2.567 − 2 |
| 38 | 21 | 1.658 − 1 | −9.018 + 0 | 5.519 − 2 |
| 38 | 20 | −9.151 − 1 | −3.799 + 0 | 1.090 − 1 |
| 38 | 19 | −1.741 + 0 | −1.122 + 0 | 1.669 − 1 |
| 38 | 18 | −1.131 + 0 | −2.849 + 0 | 1.205 − 1 |
| 38 | 17 | −1.958 + 0 | 7.161 − 1 | 1.703 − 1 |
| 38 | 16 | −2.156 + 0 | 1.986 + 0 | 1.781 − 1 |
| 38 | 15 | −8.241 − 1 | −3.804 + 0 | 1.043 − 1 |
| 38 | 14 | −3.473 − 1 | −5.139 + 0 | 6.851 − 2 |
| 38 | 13 | −3.066 + 0 | 6.274 + 0 | 2.283 − 1 |
| 38 | 12 | −3.249 + 0 | 6.430 + 0 | 2.469 − 1 |
| 38 | 11 | −2.709 + 0 | 4.772 + 0 | 2.060 − 1 |
| 38 | 10 | −3.432 + 0 | 7.195 + 0 | 2.533 − 1 |
| 38 | 9 | −5.763 + 0 | 1.593 + 1 | 4.010 − 1 |
| 38 | 8 | −4.620 + 0 | 1.044 + 1 | 3.401 − 1 |
| 38 | 7 | −6.586 + 0 | 1.817 + 1 | 4.532 − 1 |
| 38 | 6 | −7.409 + 0 | 2.051 + 1 | 5.125 − 1 |
| 38 | 5 | −5.230 + 0 | 1.040 + 1 | 3.895 − 1 |
| 38 | 4 | −6.901 + 0 | 1.652 + 1 | 4.943 − 1 |
| 38 | 3 | −6.512 + 0 | 1.415 + 1 | 4.765 − 1 |
| 38 | 2 | −4.452 + 0 | 5.279 + 0 | 3.538 − 1 |
| 38 | 1 | −6.047 + 0 | 1.299 + 1 | 4.342 − 1 |
| 38 | 0 | −2.160 + 0 | −3.408 + 0 | 2.020 − 1 |
| 39 | 39 | 2.512 + 0 | −9.352 + 0 | 3.057 − 1 |
| 39 | 38 | −1.029 + 1 | 3.435 + 1 | 8.758 − 1 |
| 39 | 37 | −1.430 + 1 | 5.646 + 1 | 9.654 − 1 |
| 39 | 36 | −9.118 + 0 | 3.673 + 1 | 6.046 − 1 |
| 39 | 35 | −3.952 + 0 | 1.590 + 1 | 2.729 − 1 |
| 39 | 34 | −2.413 + 0 | 9.103 + 0 | 1.709 − 1 |
| 39 | 33 | −2.362 − 1 | −7.707 − 1 | 4.202 − 2 |
| 39 | 32 | 2.317 + 0 | −1.215 + 1 | −1.088 − 1 |
| 39 | 31 | 4.802 + 0 | −2.309 + 1 | −2.590 − 1 |
| 39 | 30 | 4.205 + 0 | −2.212 + 1 | −2.103 − 1 |
| 39 | 29 | 4.792 + 0 | −2.490 + 1 | −2.490 − 1 |
| 39 | 28 | 4.161 + 0 | −2.313 + 1 | −2.033 − 1 |
| 39 | 27 | 4.063 + 0 | −2.310 + 1 | −1.999 − 1 |
| 39 | 26 | 3.512 + 0 | −2.146 + 1 | −1.604 − 1 |
| 39 | 25 | 3.771 + 0 | −2.305 + 1 | −1.728 − 1 |
| 39 | 24 | 2.355 + 0 | −1.766 + 1 | −8.541 − 2 |
| 39 | 23 | 3.689 + 0 | −2.347 + 1 | −1.657 − 1 |
| 39 | 22 | 3.394 − 1 | −9.871 + 0 | 3.931 − 2 |
| 39 | 21 | 1.706 + 0 | −1.607 + 1 | −3.679 − 2 |
| 39 | 20 | −8.844 − 1 | −5.169 + 0 | 1.149 − 1 |
| 39 | 19 | −3.914 − 1 | −7.406 + 0 | 8.849 − 2 |
| 39 | 18 | 2.368 − 1 | −9.701 + 0 | 4.763 − 2 |
| 39 | 17 | −6.565 − 1 | −5.729 + 0 | 9.817 − 2 |
| 39 | 16 | −8.576 − 2 | −7.633 + 0 | 6.065 − 2 |
| 39 | 15 | 8.095 − 1 | −1.070 + 1 | 1.155 − 3 |
| 39 | 14 | −1.134 + 0 | −2.552 + 0 | 1.162 − 1 |
| 39 | 13 | −1.233 + 0 | −2.018 + 0 | 1.212 − 1 |
| 39 | 12 | −4.799 − 1 | −5.207 + 0 | 7.639 − 2 |
| 39 | 11 | −1.653 + 0 | −4.503 − 1 | 1.467 − 1 |
| 39 | 10 | 1.170 − 1 | −8.666 + 0 | 5.092 − 2 |
| 39 | 9 | −2.829 + 0 | 3.358 + 0 | 2.235 − 1 |
| 39 | 8 | −7.191 + 0 | 2.026 + 1 | 4.946 − 1 |
| 39 | 7 | −3.490 + 0 | 4.554 + 0 | 2.719 − 1 |
| 39 | 6 | −4.957 + 0 | 1.013 + 1 | 3.593 − 1 |
| 39 | 5 | −7.675 + 0 | 2.028 + 1 | 5.307 − 1 |
| 39 | 4 | −7.013 + 0 | 1.643 + 1 | 5.012 − 1 |
| 39 | 3 | −5.404 + 0 | 9.188 + 0 | 4.083 − 1 |
| 39 | 2 | −4.581 + 0 | 5.640 + 0 | 3.561 − 1 |
| 39 | 1 | −7.923 + 0 | 2.024 + 1 | 5.420 − 1 |
| 39 | 0 | −3.469 + 0 | 1.625 + 0 | 2.767 − 1 |
| 40 | 40 | −9.760 − 4 | 2.431 + 0 | 4.813 − 1 |
| 40 | 39 | −1.150 + 1 | 4.061 + 1 | 9.302 − 1 |
| 40 | 38 | −1.460 + 1 | 5.856 + 1 | 9.734 − 1 |
| 40 | 37 | −1.060 + 1 | 4.359 + 1 | 6.804 − 1 |
| 40 | 36 | −7.534 + 0 | 3.123 + 1 | 4.736 − 1 |
| 40 | 35 | −2.914 + 0 | 1.120 + 1 | 1.958 − 1 |

**Table A1** (*Continued.*)

| $\nu_i$ | $\nu_f$ | $a1$ | $a2$ | $a3$ |
|---|---|---|---|---|
| 40 | 34 | −1.615 + 0 | 5.780 + 0 | 1.043 − 1 |
| 40 | 33 | 2.249 + 0 | −1.187 + 1 | −1.123 − 1 |
| 40 | 32 | 5.376 + 0 | −2.539 + 1 | −3.019 − 1 |
| 40 | 31 | 4.519 + 0 | −2.262 + 1 | −2.512 − 1 |
| 40 | 30 | 5.353 + 0 | −2.754 + 1 | −2.844 − 1 |
| 40 | 29 | 5.287 + 0 | −2.739 + 1 | −2.884 − 1 |
| 40 | 28 | 5.461 + 0 | −2.890 + 1 | −2.907 − 1 |
| 40 | 27 | 6.030 + 0 | −3.195 + 1 | −3.228 − 1 |
| 40 | 26 | 3.251 + 0 | −2.092 + 1 | −1.532 − 1 |
| 40 | 25 | 4.445 + 0 | −2.616 + 1 | −2.259 − 1 |
| 40 | 24 | 2.659 + 0 | −1.951 + 1 | −1.103 − 1 |
| 40 | 23 | 1.476 + 0 | −1.453 + 1 | −4.292 − 2 |
| 40 | 22 | 2.973 + 0 | −2.150 + 1 | −1.248 − 1 |
| 40 | 21 | 1.203 + 0 | −1.436 + 1 | −1.711 − 2 |
| 40 | 20 | −5.684 − 2 | −9.141 + 0 | 5.888 − 2 |
| 40 | 19 | 2.055 + 0 | −1.773 + 1 | −6.828 − 2 |
| 40 | 18 | 4.506 − 1 | −1.159 + 1 | 3.392 − 2 |
| 40 | 17 | 1.213 + 0 | −1.415 + 1 | −1.848 − 2 |
| 40 | 16 | −4.861 − 1 | −6.458 + 0 | 7.859 − 2 |
| 40 | 15 | 1.490 + 0 | −1.450 + 1 | −4.077 − 2 |
| 40 | 14 | 8.669 − 1 | −1.155 + 1 | −5.335 − 3 |
| 40 | 13 | 1.812 + 0 | −1.501 + 1 | −6.737 − 2 |
| 40 | 12 | −2.688 + 0 | 3.723 + 0 | 1.980 − 1 |
| 40 | 11 | −1.780 + 0 | −2.844 − 1 | 1.452 − 1 |
| 40 | 10 | −1.009 + 0 | −4.183 + 0 | 1.048 − 1 |
| 40 | 9 | −4.124 + 0 | 8.125 + 0 | 2.938 − 1 |
| 40 | 8 | −2.869 + 0 | 2.153 + 0 | 2.241 − 1 |
| 40 | 7 | −4.245 + 0 | 7.158 + 0 | 3.100 − 1 |
| 40 | 6 | −5.603 + 0 | 1.218 + 1 | 3.919 − 1 |
| 40 | 5 | −3.939 + 0 | 4.131 + 0 | 3.031 − 1 |
| 40 | 4 | −6.418 + 0 | 1.327 + 1 | 4.591 − 1 |
| 40 | 3 | −6.648 + 0 | 1.438 + 1 | 4.664 − 1 |
| 40 | 2 | −4.377 + 0 | 4.545 + 0 | 3.351 − 1 |
| 40 | 1 | −5.083 + 0 | 8.067 + 0 | 3.663 − 1 |
| 40 | 0 | −6.382 + 0 | 1.331 + 1 | 4.421 − 1 |
| 41 | 41 | −9.198 − 1 | 6.385 + 0 | 4.994 − 1 |
| 41 | 40 | −1.208 + 1 | 4.395 + 1 | 9.611 − 1 |
| 41 | 39 | −1.593 + 1 | 6.500 + 1 | 1.035 + 0 |
| 41 | 38 | −1.054 + 1 | 4.399 + 1 | 6.707 − 1 |
| 41 | 37 | −6.531 + 0 | 2.699 + 1 | 4.107 − 1 |
| 41 | 36 | −3.801 + 0 | 1.529 + 1 | 2.381 − 1 |
| 41 | 35 | −1.177 + 0 | 3.663 + 0 | 7.732 − 2 |
| 41 | 34 | 1.895 + 0 | −1.003 + 1 | −1.067 − 1 |
| 41 | 33 | 4.840 + 0 | −2.318 + 1 | −2.772 − 1 |
| 41 | 32 | 4.361 + 0 | −2.159 + 1 | −2.538 − 1 |
| 41 | 31 | 5.607 + 0 | −2.782 + 1 | −3.222 − 1 |
| 41 | 30 | 6.508 + 0 | −3.283 + 1 | −3.639 − 1 |
| 41 | 29 | 6.522 + 0 | −3.305 + 1 | −3.718 − 1 |
| 41 | 28 | 7.055 + 0 | −3.606 + 1 | −3.956 − 1 |
| 41 | 27 | 4.463 + 0 | −2.612 + 1 | −2.352 − 1 |
| 41 | 26 | 5.401 + 0 | −3.054 + 1 | −2.872 − 1 |
| 41 | 25 | 5.700 + 0 | −3.223 + 1 | −3.024 − 1 |
| 41 | 24 | 3.913 + 0 | −2.507 + 1 | −1.952 − 1 |
| 41 | 23 | 4.950 + 0 | −2.955 + 1 | −2.563 − 1 |
| 41 | 22 | 2.736 + 0 | −2.085 + 1 | −1.186 − 1 |
| 41 | 21 | 3.714 + 0 | −2.522 + 1 | −1.746 − 1 |
| 41 | 20 | 5.907 + 0 | −3.388 + 1 | −3.110 − 1 |
| 41 | 19 | 1.428 + 0 | −1.595 + 1 | −3.571 − 2 |
| 41 | 18 | 2.848 + 0 | −2.155 + 1 | −1.230 − 1 |
| 41 | 17 | 2.860 + 0 | −2.145 + 1 | −1.252 − 1 |
| 41 | 16 | 2.555 − 1 | −9.979 + 0 | 2.607 − 2 |
| 41 | 15 | 3.321 + 0 | −2.195 + 1 | −1.637 − 1 |
| 41 | 14 | 1.576 + 0 | −1.482 + 1 | −5.558 − 2 |
| 41 | 13 | 1.881 + 0 | −1.594 + 1 | −7.526 − 2 |
| 41 | 12 | 1.649 + 0 | −1.529 + 1 | −6.010 − 2 |
| 41 | 11 | −1.044 + 0 | −4.267 + 0 | 9.804 − 2 |
| 41 | 10 | −4.479 − 1 | −6.696 + 0 | 5.896 − 2 |
| 41 | 9 | −2.306 + 0 | 2.045 − 1 | 1.746 − 1 |
| 41 | 8 | −4.275 + 0 | 8.130 + 0 | 2.893 − 1 |
| 41 | 7 | −4.248 + 0 | 7.335 + 0 | 2.909 − 1 |
| 41 | 6 | −5.605 + 0 | 1.160 + 1 | 3.849 − 1 |
| 41 | 5 | −4.174 + 0 | 4.808 + 0 | 3.027 − 1 |
| 41 | 4 | −4.762 + 0 | 6.263 + 0 | 3.487 − 1 |
| 41 | 3 | −7.403 + 0 | 1.640 + 1 | 5.108 − 1 |
| 41 | 2 | −6.148 + 0 | 1.131 + 1 | 4.338 − 1 |

**Table A1** (*Continued.*)

| $\nu_i$ | $\nu_f$ | $a1$ | $a2$ | $a3$ |
|---|---|---|---|---|
| 41 | 1 | −5.223 + 0 | 7.775 + 0 | 3.732 − 1 |
| 41 | 0 | −6.466 + 0 | 1.286 + 1 | 4.454 − 1 |
| 42 | 42 | 2.145 − 1 | 5.072 + 0 | 4.611 − 1 |
| 42 | 41 | −1.246 + 1 | 4.640 + 1 | 9.705 − 1 |
| 42 | 40 | −1.449 + 1 | 5.953 + 1 | 9.457 − 1 |
| 42 | 39 | −1.126 + 1 | 4.670 + 1 | 7.029 − 1 |
| 42 | 38 | −7.724 + 0 | 3.098 + 1 | 4.869 − 1 |
| 42 | 37 | −5.588 + 0 | 2.195 + 1 | 3.378 − 1 |
| 42 | 36 | −3.688 + 0 | 1.322 + 1 | 2.222 − 1 |
| 42 | 35 | 5.925 − 1 | −5.051 + 0 | −3.778 − 2 |
| 42 | 34 | 1.730 + 0 | −1.008 + 1 | −1.170 − 1 |
| 42 | 33 | 4.054 + 0 | −2.059 + 1 | −2.491 − 1 |
| 42 | 32 | 4.548 + 0 | −2.357 + 1 | −2.731 − 1 |
| 42 | 31 | 6.863 + 0 | −3.328 + 1 | −4.204 − 1 |
| 42 | 30 | 5.904 + 0 | −3.089 + 1 | −3.436 − 1 |
| 42 | 29 | 8.460 + 0 | −4.195 + 1 | −5.002 − 1 |
| 42 | 28 | 8.905 + 0 | −4.435 + 1 | −5.212 − 1 |
| 42 | 27 | 6.445 + 0 | −3.429 + 1 | −3.792 − 1 |
| 42 | 26 | 8.043 + 0 | −4.222 + 1 | −4.582 − 1 |
| 42 | 25 | 7.076 + 0 | −3.805 + 1 | −4.082 − 1 |
| 42 | 24 | 5.059 + 0 | −3.032 + 1 | −2.824 − 1 |
| 42 | 23 | 5.486 + 0 | −3.226 + 1 | −3.079 − 1 |
| 42 | 22 | 6.752 + 0 | −3.814 + 1 | −3.747 − 1 |
| 42 | 21 | 3.405 + 0 | −2.489 + 1 | −1.683 − 1 |
| 42 | 20 | 2.344 + 0 | −1.994 + 1 | −1.133 − 1 |
| 42 | 19 | 3.088 + 0 | −2.355 + 1 | −1.498 − 1 |
| 42 | 18 | 1.429 + 0 | −1.579 + 1 | −6.124 − 2 |
| 42 | 17 | 3.072 + 0 | −2.259 + 1 | −1.596 − 1 |
| 42 | 16 | 3.295 + 0 | −2.306 + 1 | −1.752 − 1 |
| 42 | 15 | 1.183 + 0 | −1.325 + 1 | −6.135 − 2 |
| 42 | 14 | 1.951 + 0 | −1.617 + 1 | −1.097 − 1 |
| 42 | 13 | 1.451 + 0 | −1.401 + 1 | −7.901 − 2 |
| 42 | 12 | 8.564 − 1 | −1.202 + 1 | −4.038 − 2 |
| 42 | 11 | 9.626 − 1 | −1.326 + 1 | −3.926 − 2 |
| 42 | 10 | −1.122 + 0 | −5.608 + 0 | 9.380 − 2 |
| 42 | 9 | −2.039 + 0 | −2.013 + 0 | 1.461 − 1 |
| 42 | 8 | −5.209 + 0 | 1.077 + 1 | 3.350 − 1 |
| 42 | 7 | −4.701 + 0 | 8.179 + 0 | 3.057 − 1 |
| 42 | 6 | −6.544 + 0 | 1.455 + 1 | 4.259 − 1 |
| 42 | 5 | −5.423 + 0 | 9.269 + 0 | 3.584 − 1 |
| 42 | 4 | −4.773 + 0 | 5.529 + 0 | 3.304 − 1 |
| 42 | 3 | −4.249 + 0 | 3.630 + 0 | 2.898 − 1 |
| 42 | 2 | −5.210 + 0 | 7.486 + 0 | 3.473 − 1 |
| 42 | 1 | −5.620 + 0 | 9.386 + 0 | 3.689 − 1 |
| 42 | 0 | −6.618 + 0 | 1.346 + 1 | 4.280 − 1 |
| 43 | 43 | −3.813 + 0 | 2.035 + 1 | 6.874 − 1 |
| 43 | 42 | −9.478 + 0 | 3.467 + 1 | 7.997 − 1 |
| 43 | 41 | −1.222 + 1 | 4.957 + 1 | 8.033 − 1 |
| 43 | 40 | −1.034 + 1 | 4.210 + 1 | 6.570 − 1 |
| 43 | 39 | −9.103 + 0 | 3.665 + 1 | 5.518 − 1 |
| 43 | 38 | −7.092 + 0 | 2.717 + 1 | 4.323 − 1 |
| 43 | 37 | −6.104 + 0 | 2.231 + 1 | 3.601 − 1 |
| 43 | 36 | −1.855 + 0 | 3.897 + 0 | 1.052 − 1 |
| 43 | 35 | −8.243 − 2 | −3.662 + 0 | −9.612 − 3 |
| 43 | 34 | 2.220 + 0 | −1.302 + 1 | −1.648 − 1 |
| 43 | 33 | 3.198 + 0 | −1.848 + 1 | −2.059 − 1 |
| 43 | 32 | 3.753 + 0 | −2.143 + 1 | −2.388 − 1 |
| 43 | 31 | 6.119 + 0 | −3.106 + 1 | −3.929 − 1 |
| 43 | 30 | 7.803 + 0 | −3.967 + 1 | −4.732 − 1 |
| 43 | 29 | 7.990 + 0 | −4.089 + 1 | −4.845 − 1 |
| 43 | 28 | 7.904 + 0 | −4.136 + 1 | −4.743 − 1 |
| 43 | 27 | 7.940 + 0 | −4.145 + 1 | −4.817 − 1 |
| 43 | 26 | 7.407 + 0 | −4.024 + 1 | −4.403 − 1 |
| 43 | 25 | 7.019 + 0 | −3.911 + 1 | −4.135 − 1 |
| 43 | 24 | 8.207 + 0 | −4.412 + 1 | −4.861 − 1 |
| 43 | 23 | 6.202 + 0 | −3.611 + 1 | −3.653 − 1 |
| 43 | 22 | 4.526 + 0 | −2.986 + 1 | −2.562 − 1 |
| 43 | 21 | 4.039 + 0 | −2.708 + 1 | −2.419 − 1 |
| 43 | 20 | 3.922 + 0 | −2.707 + 1 | −2.302 − 1 |
| 43 | 19 | 9.806 − 1 | −1.479 + 1 | −5.687 − 2 |
| 43 | 18 | 3.922 + 0 | −2.700 + 1 | −2.294 − 1 |
| 43 | 17 | 6.288 − 1 | −1.335 + 1 | −3.478 − 2 |
| 43 | 16 | 1.296 + 0 | −1.532 + 1 | −8.229 − 2 |
| 43 | 15 | −1.105 − 1 | −9.159 + 0 | −6.561 − 4 |
| 43 | 14 | 3.007 + 0 | −2.125 + 1 | −1.943 − 1 |

**Table A1** (*Continued.*)

| $\nu_i$ | $\nu_f$ | $a1$ | $a2$ | $a3$ |
|---|---|---|---|---|
| 43 | 13 | −5.600 − 1 | −6.371 + 0 | 1.436 − 2 |
| 43 | 12 | −8.501 − 1 | −5.982 + 0 | 4.200 − 2 |
| 43 | 11 | −2.034 + 0 | −1.387 + 0 | 1.153 − 1 |
| 43 | 10 | 9.646 − 1 | −1.479 + 1 | −5.415 − 2 |
| 43 | 9 | −3.981 − 1 | −9.910 + 0 | 3.115 − 2 |
| 43 | 8 | −2.032 + 0 | −3.399 + 0 | 1.264 − 1 |
| 43 | 7 | −4.558 + 0 | 6.586 + 0 | 2.766 − 1 |
| 43 | 6 | −8.317 + 0 | 2.136 + 1 | 5.011 − 1 |
| 43 | 5 | −5.816 + 0 | 1.014 + 1 | 3.548 − 1 |
| 43 | 4 | −6.122 + 0 | 1.196 + 1 | 3.611 − 1 |
| 43 | 3 | −4.728 + 0 | 5.809 + 0 | 2.780 − 1 |
| 43 | 2 | −3.958 + 0 | 1.907 + 0 | 2.375 − 1 |
| 43 | 1 | −7.824 + 0 | 1.896 + 1 | 4.531 − 1 |
| 43 | 0 | −7.991 + 0 | 2.030 + 1 | 4.565 − 1 |
| 44 | 44 | −5.640 − 1 | 1.369 + 1 | 5.794 − 1 |
| 44 | 43 | −7.954 + 0 | 2.877 + 1 | 7.045 − 1 |
| 44 | 42 | −9.406 + 0 | 3.566 + 1 | 6.691 − 1 |
| 44 | 41 | −1.164 + 1 | 4.412 + 1 | 7.505 − 1 |
| 44 | 40 | −1.198 + 1 | 4.458 + 1 | 7.670 − 1 |
| 44 | 39 | −1.141 + 1 | 4.134 + 1 | 7.081 − 1 |
| 44 | 38 | −1.184 + 1 | 4.267 + 1 | 7.298 − 1 |
| 44 | 37 | −8.649 + 0 | 2.870 + 1 | 5.232 − 1 |
| 44 | 36 | −4.665 + 0 | 1.227 + 1 | 2.730 − 1 |
| 44 | 35 | −3.471 + 0 | 7.588 + 0 | 1.874 − 1 |
| 44 | 34 | −1.565 − 1 | −6.556 + 0 | −1.982 − 2 |
| 44 | 33 | −1.446 + 0 | −1.992 + 0 | 6.174 − 2 |
| 44 | 32 | 5.633 + 0 | −3.163 + 1 | −3.625 − 1 |
| 44 | 31 | 3.860 + 0 | −2.530 + 1 | −2.557 − 1 |
| 44 | 30 | 6.402 + 0 | −3.588 + 1 | −4.090 − 1 |
| 44 | 29 | 5.349 + 0 | −3.170 + 1 | −3.536 − 1 |
| 44 | 28 | 6.400 + 0 | −3.780 + 1 | −3.955 − 1 |
| 44 | 27 | 6.273 + 0 | −3.719 + 1 | −3.980 − 1 |
| 44 | 26 | 7.134 + 0 | −4.080 + 1 | −4.543 − 1 |
| 44 | 25 | 3.031 + 0 | −2.483 + 1 | −2.010 − 1 |
| 44 | 24 | 3.959 + 0 | −2.845 + 1 | −2.622 − 1 |
| 44 | 23 | 6.394 + 0 | −3.896 + 1 | −4.085 − 1 |
| 44 | 22 | 5.061 + 0 | −3.374 + 1 | −3.276 − 1 |
| 44 | 21 | 1.855 + 0 | −2.070 + 1 | −1.360 − 1 |
| 44 | 20 | 4.335 + 0 | −3.113 + 1 | −2.824 − 1 |
| 44 | 19 | 3.237 + 0 | −2.645 + 1 | −2.218 − 1 |
| 44 | 18 | 3.741 + 0 | −2.861 + 1 | −2.526 − 1 |
| 44 | 17 | 2.425 − 1 | −1.377 + 1 | −5.188 − 2 |
| 44 | 16 | 2.931 + 0 | −2.490 + 1 | −2.080 − 1 |
| 44 | 15 | −5.958 − 1 | −9.615 + 0 | −5.667 − 3 |
| 44 | 14 | 2.299 + 0 | −1.985 + 1 | −2.011 − 1 |
| 44 | 13 | −4.449 − 1 | −9.850 + 0 | −1.872 − 2 |
| 44 | 12 | −1.045 + 0 | −6.695 + 0 | 6.723 − 3 |
| 44 | 11 | 1.890 − 1 | −1.246 + 1 | −6.245 − 2 |
| 44 | 10 | 1.367 + 0 | −1.855 + 1 | −1.177 − 1 |
| 44 | 9 | 1.631 + 0 | −1.965 + 1 | −1.364 − 1 |
| 44 | 8 | −1.416 + 0 | −7.979 + 0 | 4.577 − 2 |
| 44 | 7 | −7.298 + 0 | 1.646 + 1 | 3.852 − 1 |
| 44 | 6 | −2.434 + 0 | −4.815 + 0 | 1.043 − 1 |
| 44 | 5 | −7.527 + 0 | 1.599 + 1 | 4.006 − 1 |
| 44 | 4 | −7.526 + 0 | 1.458 + 1 | 4.168 − 1 |
| 44 | 3 | −5.091 + 0 | 4.728 + 0 | 2.612 − 1 |
| 44 | 2 | −9.400 + 0 | 2.200 + 1 | 5.216 − 1 |
| 44 | 1 | −9.242 + 0 | 2.253 + 1 | 4.932 − 1 |
| 44 | 0 | −1.179 + 1 | 3.302 + 1 | 6.494 − 1 |
| 45 | 45 | −1.667 + 0 | 1.266 + 1 | 5.645 − 1 |
| 45 | 44 | −6.557 + 0 | 2.461 + 1 | 6.307 − 1 |
| 45 | 43 | −1.140 + 1 | 4.249 + 1 | 7.782 − 1 |
| 45 | 42 | −1.235 + 1 | 4.362 + 1 | 8.546 − 1 |
| 45 | 41 | −1.155 + 1 | 3.921 + 1 | 7.657 − 1 |
| 45 | 40 | −9.457 + 0 | 2.986 + 1 | 6.397 − 1 |
| 45 | 39 | −8.282 + 0 | 2.497 + 1 | 5.300 − 1 |
| 45 | 38 | −9.360 + 0 | 2.913 + 1 | 5.869 − 1 |
| 45 | 37 | −7.502 + 0 | 2.107 + 1 | 4.582 − 1 |
| 45 | 36 | −6.212 + 0 | 1.456 + 1 | 3.833 − 1 |
| 45 | 35 | −5.954 + 0 | 1.385 + 1 | 3.504 − 1 |
| 45 | 34 | −4.412 + 0 | 7.018 + 0 | 2.486 − 1 |
| 45 | 33 | −3.869 + 0 | 3.516 + 0 | 2.260 − 1 |
| 45 | 32 | −1.009 + 0 | −8.868 + 0 | 5.233 − 2 |
| 45 | 31 | 5.998 − 1 | −1.499 + 1 | −6.781 − 2 |
| 45 | 30 | −4.815 + 0 | 6.531 + 0 | 2.612 − 1 |

**Table A1** (*Continued.*)

| $\nu_i$ | $\nu_f$ | $a1$ | $a2$ | $a3$ |
|---|---|---|---|---|
| 45 | 29 | −2.808 + 0 | −2.276 + 0 | 1.359 − 1 |
| 45 | 28 | −7.224 − 1 | −1.287 + 1 | 3.477 − 2 |
| 45 | 27 | −5.234 − 4 | −1.572 + 1 | −2.192 − 2 |
| 45 | 26 | −1.652 + 0 | −9.258 + 0 | 7.456 − 2 |
| 45 | 25 | −5.328 + 0 | 5.533 + 0 | 2.907 − 1 |
| 45 | 24 | 2.254 + 0 | −2.640 + 1 | −1.593 − 1 |
| 45 | 23 | −3.185 + 0 | −4.005 + 0 | 1.587 − 1 |
| 45 | 22 | −2.900 − 1 | −1.612 + 1 | −1.355 − 2 |
| 45 | 21 | −2.656 + 0 | −6.524 + 0 | 1.280 − 1 |
| 45 | 20 | 8.739 − 1 | −1.976 + 1 | −1.042 − 1 |
| 45 | 19 | 5.624 − 1 | −1.890 + 1 | −8.575 − 2 |
| 45 | 18 | −7.978 − 1 | −1.443 + 1 | 1.268 − 2 |
| 45 | 17 | −2.483 + 0 | −6.312 + 0 | 9.442 − 2 |
| 45 | 16 | −4.962 + 0 | 4.860 + 0 | 2.305 − 1 |
| 45 | 15 | 6.239 − 1 | −1.740 + 1 | −1.119 − 1 |
| 45 | 14 | −2.486 + 0 | −4.154 + 0 | 6.506 − 2 |
| 45 | 13 | −2.534 + 0 | −3.222 + 0 | 5.670 − 2 |
| 45 | 12 | 2.670 + 0 | −2.547 + 1 | −2.439 − 1 |
| 45 | 11 | 2.010 + 0 | −2.160 + 1 | −2.225 − 1 |
| 45 | 10 | 3.251 + 0 | −2.864 + 1 | −2.743 − 1 |
| 45 | 9 | −1.725 + 0 | −8.185 + 0 | 2.078 − 2 |
| 45 | 8 | 1.571 + 0 | −2.123 + 1 | −1.906 − 1 |
| 45 | 7 | −1.295 + 0 | −1.052 + 1 | −1.562 − 2 |
| 45 | 6 | −4.565 + 0 | 1.493 + 0 | 1.901 − 1 |
| 45 | 5 | −4.267 − 1 | −1.635 + 1 | −5.551 − 2 |
| 45 | 4 | −2.487 + 0 | −9.388 + 0 | 8.919 − 2 |
| 45 | 3 | −2.229 + 0 | −1.022 + 1 | 6.065 − 2 |
| 45 | 2 | −4.831 − 2 | −2.090 + 1 | −5.300 − 2 |
| 45 | 1 | −7.743 + 0 | 1.143 + 1 | 3.971 − 1 |
| 45 | 0 | −6.064 + 0 | 6.111 + 0 | 2.720 − 1 |
| 46 | 46 | −2.659 + 0 | 1.771 + 1 | 6.436 − 1 |
| 46 | 45 | −4.604 + 0 | 1.659 + 1 | 5.353 − 1 |
| 46 | 44 | −8.383 + 0 | 2.749 + 1 | 6.616 − 1 |
| 46 | 43 | −7.570 + 0 | 2.619 + 1 | 4.550 − 1 |
| 46 | 42 | −2.956 + 0 | 8.192 + 0 | 1.419 − 1 |
| 46 | 41 | 1.018 + 0 | −9.118 + 0 | −1.330 − 1 |
| 46 | 40 | 5.570 + 0 | −2.868 + 1 | −3.956 − 1 |
| 46 | 39 | 6.781 + 0 | −3.518 + 1 | −4.819 − 1 |
| 46 | 38 | 1.094 + 1 | −5.572 + 1 | −6.888 − 1 |
| 46 | 37 | 1.152 + 1 | −6.134 + 1 | −7.078 − 1 |
| 46 | 36 | 7.862 + 0 | −4.861 + 1 | −4.710 − 1 |
| 46 | 35 | 7.064 + 0 | −4.768 + 1 | −4.055 − 1 |
| 46 | 34 | 5.687 + 0 | −4.372 + 1 | −3.181 − 1 |
| 46 | 33 | 6.431 + 0 | −4.980 + 1 | −3.333 − 1 |
| 46 | 32 | −1.571 + 0 | −1.788 + 1 | 1.491 − 1 |
| 46 | 31 | −6.556 + 0 | 2.349 + 0 | 4.317 − 1 |
| 46 | 30 | −1.321 + 1 | 2.697 + 1 | 8.595 − 1 |
| 46 | 29 | −1.671 + 1 | 4.261 + 1 | 1.032 + 0 |
| 46 | 28 | −1.429 + 1 | 3.143 + 1 | 9.047 − 1 |
| 46 | 27 | −1.715 + 1 | 4.223 + 1 | 1.068 + 0 |
| 46 | 26 | −1.921 + 1 | 5.070 + 1 | 1.183 + 0 |
| 46 | 25 | −2.004 + 1 | 5.440 + 1 | 1.221 + 0 |
| 46 | 24 | −2.029 + 1 | 5.643 + 1 | 1.213 + 0 |
| 46 | 23 | −2.684 + 1 | 8.275 + 1 | 1.607 + 0 |
| 46 | 22 | −2.159 + 1 | 6.080 + 1 | 1.296 + 0 |
| 46 | 21 | −2.343 + 1 | 7.042 + 1 | 1.368 + 0 |
| 46 | 20 | −2.051 + 1 | 5.657 + 1 | 1.213 + 0 |
| 46 | 19 | −1.864 + 1 | 5.081 + 1 | 1.072 + 0 |
| 46 | 18 | −2.174 + 1 | 6.272 + 1 | 1.260 + 0 |
| 46 | 17 | −2.266 + 1 | 6.933 + 1 | 1.283 + 0 |
| 46 | 16 | −1.355 + 1 | 3.113 + 1 | 7.378 − 1 |
| 46 | 15 | −2.106 + 1 | 6.400 + 1 | 1.163 + 0 |
| 46 | 14 | −1.441 + 1 | 3.748 + 1 | 7.539 − 1 |
| 46 | 13 | −2.109 + 1 | 6.612 + 1 | 1.138 + 0 |
| 46 | 12 | −1.615 + 1 | 4.525 + 1 | 8.408 − 1 |
| 46 | 11 | −1.452 + 1 | 3.847 + 1 | 7.456 − 1 |
| 46 | 10 | −1.291 + 1 | 3.212 + 1 | 6.369 − 1 |
| 46 | 9 | −9.698 + 0 | 1.847 + 1 | 4.534 − 1 |
| 46 | 8 | −3.634 + 0 | −6.609 + 0 | 7.543 − 2 |
| 46 | 7 | −1.617 + 1 | 4.404 + 1 | 8.372 − 1 |
| 46 | 6 | −1.633 + 1 | 4.502 + 1 | 8.238 − 1 |
| 46 | 5 | −2.005 + 1 | 5.784 + 1 | 1.073 + 0 |
| 46 | 4 | −3.065 + 1 | 1.032 + 2 | 1.669 + 0 |
| 46 | 3 | −7.430 + 0 | 8.064 + 0 | 2.713 − 1 |
| 46 | 2 | −8.864 + 0 | 1.587 + 1 | 3.359 − 1 |

**Table A1** (*Continued.*)

| $\nu_i$ | $\nu_f$ | $a1$ | $a2$ | $a3$ |
|---|---|---|---|---|
| 46 | 1 | $-1.030+1$ | $1.995+1$ | $4.368-1$ |
| 46 | 0 | $-3.801+1$ | $1.309+2$ | $2.147+0$ |

## References


[1] Capitelli, M., Colonna, G., and Esposito, F., "On the Coupling of Vibrational Relaxation with the Dissociation-Recombination Kinetics: From Dynamics to Aerospace Applications," *Journal of Physical Chemistry A*, Vol. 108, No. 41, 2004, pp. 8930–8934. doi:10.1021/jp048847v

[2] Laux, C. O., Pierrot, L., and Gessman, R. J., "State-to-State Modeling of a Recombining Nitrogen Plasma Experiment," *Chemical Physics*, Vol. 398, April 2012, pp. 46–55. doi:10.1016/j.chemphys.2011.10.028

[3] Panesi, M., Jaffe, R. L., Schwenke, D. W., and Magin, T. E., "Rovibrational Internal Energy Transfer and Dissociation of $N_2(^1\Sigma_g^+) - N(^4S_u)$ System in Hypersonic Flows," *Journal of Chemical Physics*, Vol. 138, No. 4, 2013, Paper 044312. doi:10.1063/1.4774412

[4] Kim, J. G., and Boyd, I. D., "State-Resolved Master Equation Analysis of Thermochemical Nonequilibrium of Nitrogen," *Chemical Physics*, Vol. 415, March 2013, pp. 237–246. doi:10.1016/j.chemphys.2013.01.027

[5] Esposito, F., Armenise, I., Capitta, G., and Capitelli, M., "$O + O_2$ State-to-State Vibrational Relaxation and Dissociation Rates Based on Quasiclassical Calculations," *Chemical Physics*, Vol. 351, July 2008, pp. 91–98. doi:10.1016/j.chemphys.2008.04.004

[6] Armenise, I., and Esposito, F., "N 2, o 2, No State-to-State Vibrational Kinetics in Hypersonic Boundary Layers: The Problem of Rescaling Rate Coefficients to Uniform Vibrational Ladders," *Chemical Physics*, Vol. 446, 2015, pp. 30–46. doi:10.1016/j.chemphys.2014.11.004

[7] Kim, J. G., Kwon, O. J., and Park, C., "Master Equation Study and Nonequilibrium Chemical Reactions for H + H and He + H," *Journal of Thermophysics and Heat Transfer*, Vol. 23, No. 3, July 2009, pp. 443–453. doi:10.2514/1.41741

[8] Bose, D., and Candler, G. V., "Thermal Rate Constants of the n2+ o no+ n Reaction Using Abinitio3a and 3a Potential Energy Surfaces," *Journal of Chemical Physics*, Vol. 104, No. 8, 1996, pp. 2825–2833. doi:10.1063/1.471106

[9] Esposito, F., Capitelli, M., and Gorse, C., "Quasi-Classical Dynamics and Vibrational Kinetics of n+ n 2 (v) System," *Chemical Physics*, Vol. 257, No. 2, 2000, pp. 193–202. doi:10.1016/S0301-0104(00)00155-5

[10] Kim, J. G., and Boyd, I. D., "Thermochemical Nonequilibirum Modeling of Electronically Excited Molecular Oxygen," *11th AIAA/ASME Joint Thermophysics and Heat Transfer Conference*, AIAA Paper 2014-2963, 2014.

[11] Esposito, F., and Capitelli, M., "The Relaxation of Vibrationally Excited $O_2$ Molecules by Atomic Oxygen," *Chemical Physics Letters*, Vol. 443, No. 4, 2007, pp. 222–226. doi:10.1016/j.cplett.2007.06.099

[12] Quack, M., and Troe, J., "Complex Formation in Reactive and Inelastic Scattering: Statistical Adiabatic Channel Model of Unimolecular Processes III," *Berichte der Bunsengesellschaft für Physikalische Chemie*, Vol. 79, No. 2, 1975, pp. 170–183. doi:10.1002/bbpc.19750790211

[13] Varandas, A., and Pais, A., "A Realistic Double Many-Body Expansion (DMBE) Potential Energy Surface for Ground-State $O_3$ from a Multiproperty Fit to Ab Initio Calculations, and to Experimental Spectroscopic, Inelastic Scattering, and Kinetic Isotope Thermal Rate Data," *Molecular Physics*, Vol. 65, Nov. 1988, pp. 843–860. doi:10.1080/00268978800101451

[14] Neitzel, K., Andrienko, D., and Boyd, I. D., "Modeling Fidelity for Oxygen Nonequilibrium Thermochemistry in Reflected Shock Tube Flows," *45th AIAA Thermophysics Conference*, AIAA Paper 2015-2509, June 2015.

[15] Ibraguimova, L., Sergievskaya, A., Levashov, V. Y., Shatalov, O., Tunik, Y. V., and Zabelinskii, I., "Investigation of Oxygen Dissociation and Vibrational Relaxation at Temperatures 4000–10 800 k," *Journal of Chemical Physics*, Vol. 139, No. 3, 2013, Paper 034317. doi:10.1063/1.4813070

[16] Adamovich, I. V., MacHeret, S. O., Rich, J. W., and Treanor, C. E., "Vibrational Energy Transfer Rates Using a Forced Harmonic Oscillator Model," *Journal of Thermophysics and Heat Transfer*, Vol. 12, No. 1, 1998, pp. 57–65. doi:10.2514/2.6302

[17] Park, C., *Nonequilibrium Hypersonic Aerothermodynamics*, Wiley, Hoboken, NJ, 1989, pp. 57–59.

[18] Steele, D., Lippincott, E. R., and Vanderslice, J. T., "Comparative Study of Empirical Internuclear Potential Functions," *Reviews of Modern Physics*, Vol. 34, No. 2, 1962, Paper 239. doi:10.1103/RevModPhys.34.239

[19] Charlo, D., and Clary, D. C., "Quantum-Mechanical Calculations on Termolecular Association Reactions xy+ z+ m xyz+ m: Application to Ozone Formation," *The Journal of Chemical Physics*, Vol. 117, No. 4, 2002, pp. 1660–1672. doi:10.1063/1.1485069

[20] Schinke, R., Grebenshchikov, S. Y., Ivanov, M., and Fleurat-Lessard, P., "Dynamical Studies of the Ozone Isotope Effect: A Status Report," *Annual Review of Physical Chemistry*, Vol. 57, Jan. 2006, pp. 625–661. doi:10.1146/annurev.physchem.57.032905.104542

[21] Herzberg, G., *Molecular Spectra and Molecular Structure*, Vol. 1, D. Van Nostrand Company Inc., Princeton, NJ, 1957, pp. 128–132.

[22] Varandas, A. J. C., and Dias de Silva, J., "Hartree–Fock Approximate Correlation Energy (Hface) Potential for Diatomic Interactions. Molecules and Van Der Waals Molecules," *Journal of the Chemical Society, Faraday Transactions 2: Molecular and Chemical Physics*, Vol. 82, No. 4, 1986, pp. 593–608. doi:10.1039/f29868200593

[23] "Vibrational Relaxation, and Dissociation of Oxygen in Molecule-Atom Collisions," *45th AIAA Thermophysics Conference*, AIAA Paper 2015-3251, June 2015.

[24] Millikan, R. C., and White, D. R., "Systematics of Vibrational Relaxation," *Journal of Chemical Physics*, Vol. 39, No. 12, 1963, Paper 3209. doi:10.1063/1.1734182

[25] Wray, K. L., "Shock-Tube Study of the Vibrational Relaxation of Nitric Oxide," *Journal of Chemical Physics*, Vol. 36, No. 10, 1962, pp. 2597–2603. doi:10.1063/1.1732339

[26] Eckstrom, D., "Vibrational Relaxation of Shock-Heated $N_2$ by Atomic Oxygen Using the ir Tracer Method," *Journal of Chemical Physics*, Vol. 59, No. 6, 1973, pp. 2787–2795. doi:10.1063/1.1680410

[27] Breen, J., Quy, R., and Glass, G., "Vibrational Relaxation of $O_2$ in the Presence of Atomic Oxygen," *Journal of Chemical Physics*, Vol. 59, No. 1, 1973, pp. 556–557. doi:10.1063/1.1679846

[28] Kiefer, J. H., and Lutz, R. W., "The Effect of Oxygen Atoms on the Vibrational Relaxation of Oxygen," *Symposium (International) on Combustion*, Vol. 11, Elsevier, New York, 1967, pp. 67–76.

[29] Pritchard, H. O., *Transfer and Storage of Energy by Molecules*, Vol. 2, edited by Burnett, G. M., and North, A. M., Wiley-Interscience, New York, 1969, pp. 368–369.

[30] Breig, E. L., "Statistical Model for the Vibrational Deactivation of Molecular by Atomic Oxygen," *Journal of Chemical Physics*, Vol. 51, No. 10, 1969, Paper 4539. doi:10.1063/1.1671825

[31] Lee, C., and Kim, H.-R., "A Classical Trajectory Study of $O + O_2$ Collision," *Chemical Physics Letters*, Vol. 233, No. 5, 1995, pp. 658–664. doi:10.1016/0009-2614(94)01509-T

[32] Andrienko, D., and Boyd, I. D., "Investigation of Oxygen Vibrational Relaxation by Quasi-Classical Trajectory Method," *Chemical Physics*, Vol. 459, Sept. 2015, pp. 1–13. doi:10.1016/j.chemphys.2015.07.023

[33] Truhlar, D. G., and Muckerman, J. T., "Reactive Scattering Cross Sections III: Quasiclassical and Semiclassical Methods," *Atom-Molecule Collision Theory*, edited by Bernstein, R. B., Plenum Press, New York, 1979, pp. 505–566.

[34] Eaker, C. W., Schatz, G. C., De Leon, N., and Heller, E. J., "Fourier Transform Methods for Calculating Action Variables and Semiclassical Eigenvalues for Coupled Oscillator Systems," *Journal of Chemical Physics*, Vol. 81, No. 12, 1984, pp. 5913–5919. doi:10.1063/1.447592

[35] Lapidus, L., and Seinfeld, J. H., *Numerical Solution of Ordinary Differential Equations*, Elsevier, New York, 1971, pp. 40–45.

[36] Gross, A., and Billing, G. D., "Isotope Effects on the Rate Constants for the Processes $O_2 + O \rightarrow O + O_2$ and $O_2 + O + Ar \rightarrow O_3 + Ar$ on a Modified Ground-State Potential Energy Surface for Ozone," *Chemical*

*Physics*, Vol. 217, No. 1, 1997, pp. 1–18.
doi:10.1016/S0301-0104(97)84555-7

[37] Zabelinskii, I., Ibraguimova, L., and Shatalov, O., "Measurement of the Vibrational Temperature of Oxygen Behind a Shock Wave Front Under Thermal and Chemical Nonequilibrium Conditions," *Fluid Dynamics*, Vol. 45, No. 3, 2010, pp. 485–492.
doi:10.1134/S0015462810030154

[38] Bender, J. D., Valentini, P., Nompelis, I., Schwartzentruber, T., and Candler, G. V., "Characterization of Vibrational and Rotational Energy Transfer in $N_2 + N_2$ Dissociative Collisions Using the Quasiclassical Trajectory Method" *45th AIAA Thermophysics Conference*, AIAA Paper 2015-3253, June 2015.

[39] Park, C., "Rotational Relaxation of $N_2$ Behind a Strong Shock Wave," *Journal of Thermophysics and Heat Transfer*, Vol. 18, No. 4, 2004, pp. 527–533.
doi:10.2514/1.11442

[40] Park, C., "Review of Chemical-Kinetic Problems of Future Nasa Missions. I—Earth Entries," *Journal of Thermophysics and Heat Transfer*, Vol. 7, No. 3, Jan. 1993, pp. 385–398.
doi:10.2514/3.431

[41] Bauer, S., and Tsang, S., "Mechanisms for Vibrational Relaxation at High Temperatures," *Physics of Fluids*, Vol. 6, No. 2, 1963, pp. 182–189.
doi:10.1063/1.1706717

[42] Kalogerakis, K. S., Copeland, R. A., and Slanger, T. G., "Measurement of the Rate Coefficient for Collisional Removal of $O_2(X^3\Sigma_g^-, \nu = 1)$ and $(a^1\Delta_g, \nu = 1)$ by $O(^3P)$," *Journal of Chemical Physics*, Vol. 123, No. 19, 2005, Paper 194303.
doi:10.1063/1.2110227

[43] Pejaković, D. A., Campbell, Z., Kalogerakis, K. S., Copeland, R. A., and Slanger, T. G., "Collisional Relaxation of $O_2(X^3\Sigma_g^-, \nu = 1)$ and $(a^1\Delta_g, \nu = 1)$ by Atmospherically Relevant Species," *Journal of Chemical Physics*, Vol. 135, No. 9, 2011.

[44] Landau, L., and Teller, E., "Theory of Sound Dispersion," *Physikalische Zeitschrift der Sowjetunion*, Vol. 10, No. 1, 1936, Paper 34.

[45] Colonna, G., Esposito, F., and Capitelli, M., "The Role of Rotation in State-to-State Vibrational Kinetics," *9th AIAA/ASME Joint Thermophysics and Heat Transfer Conference*, AIAA Paper 2006-3423, 2006.

[46] Capitelli, M., Ferreira, C. M., Osipov, A. I., and Gordiets, B. F., *Plasma Kinetics in Atmospheric Gases*, Springer, New York, 2000, pp. 5–22.

[47] Camac, M., "$O_2$ Vibration Relaxation in Oxygen-Argon Mixtures," *Journal of Chemical Physics*, Vol. 34, No. 2, 1961, pp. 448–459.
doi:10.1063/1.4757208

**This article has been cited by:**


1. Sergey F. Gimelshein, Ingrid J. Wysong, Igor V. Adamovich. Direct Simulation Monte Carlo Application of the Three-Dimensional Forced Harmonic Oscillator Model. *Journal of Thermophysics and Heat Transfer*, ahead of print1-10. [Abstract] [Full Text] [PDF] [PDF Plus]
2. Jiaao Hao, Jingying Wang, Chunhian Lee. 2017. State-specific simulation of oxygen vibrational excitation and dissociation behind a normal shock. *Chemical Physics Letters* **681**, 69-74. [Crossref]
3. Jiaao Hao, Jingying Wang, Chunhian Lee. 2017. Assessment of vibration–dissociation coupling models for hypersonic nonequilibrium simulations. *Aerospace Science and Technology* **67**, 433-442. [Crossref]
4. Matthew F. Campbell, Kyle G. Owen, David F. Davidson, Ronald K. Hanson. 2017. Dependence of Calculated Postshock Thermodynamic Variables on Vibrational Equilibrium and Input Uncertainty. *Journal of Thermophysics and Heat Transfer* **31**:3, 586-608. [Abstract] [Full Text] [PDF] [PDF Plus]
5. P. Nizenkov, M. Pfeiffer, A. Mirza, S. Fasoulas. 2017. Modeling of chemical reactions between polyatomic molecules for atmospheric entry simulations with direct simulation Monte Carlo. *Physics of Fluids* **29**:7, 077104. [Crossref]
6. Daniil A. Andrienko, Iain D. Boyd. 2016. Thermal relaxation of molecular oxygen in collisions with nitrogen atoms. *The Journal of Chemical Physics* **145**:1, 014309. [Crossref]
7. Eswar Josyula, Jonathan M. Burt, Vincenzo Laporta, Prakash Vedula. State-to-State Kinetic Modeling of Oxygen in Hypersonic Nonequilibrium Flows . [Citation] [PDF] [PDF Plus]